A peer-reviewed version of this preprint was published in PeerJ on 15 August 2018.

View the peer-reviewed version (peerj.com/articles/5387), which is the preferred citable publication unless you specifically need to cite this preprint.

Anderson EE, Wilson C, Knap AH, Villareal TA. 2018. Summer diatom blooms in the eastern North Pacific gyre investigated with a long-endurance autonomous surface vehicle. PeerJ 6:e5387 https://doi.org/10.7717/peerj.5387

PeerJ Preprints NOT PEER-REVIEWED

Summer diatom blooms in the eastern North Pacific gyre investigated with a long-endurance autonomous surface vehicle

Emily E Anderson [1] , **Cara Wilson** [2] , **Anthony H Knap** [3] , **Tracy A Villareal** Corresp. [1]

[1] Dept. of Marine Science, The University of Texas at Austin, Port Aransas, Texas, United States of America

[2] National Marine Fisheries, National Oceanic and Atmospheric Administration, Monterey, California, United States of America

[3] Texas A&M University, Geochemical and Environmental Research Group, College Station, Texas, United States of America

Corresponding Author: Tracy A Villareal
Email address: tracyv@austin.utexas.edu

Satellite chlorophyll (chl) observations have repeatedly observed summertime phytoplankton blooms in the North Pacific subtropical gyre (NPSG), a region of open ocean that is far removed from any land-derived or Ekman upwelling nutrient sources. These blooms are dominated by N_2-fixing diatom-cyanobacteria associations of the diatom genera *Rhizosolenia* Brightwell and *Hemiaulus* Ehrenberg. Their nitrogen fixing endosymbiont, *Richelia intracellularis* J.A. Schmidt, is hypothesized to be critical to the development of blooms in this nitrogen limited region. However, due to the remote location and unpredictable duration of the summer blooms, prolonged *in situ* observations are rare outside of the Station ALOHA time-series off of Hawai'i. In summer, 2015, a proof-of–concept mission using the autonomous vehicle, *Honey Badger* (Wave Glider SV2), collected near-surface (<20m) observations in the NPSG using hydrographic, meteorological, optical, and imaging sensors designed to focus on phytoplankton abundance, distribution and physiology of this bloom-forming region. *Hemiaulus* and *Rhizosolenia* cell abundance was determined using digital holography for the entire June-November mission. *Honey Badger* was not able to reach the 30°N subtropical front region where most of the satellite chl blooms have been observed, but near-real time navigational control allowed it to transect two blooms near 25°N. The two taxa did not co-occur in large numbers, rather the blooms were dominated by either *Hemiaulus* or *Rhizosolenia*. The 2-4 August 2015 bloom was comprised of 96% *Hemiaulus* and the second bloom, 15-17 August 2015, was dominated by *Rhizosolenia* (75%). The holograms also imaged undisturbed, fragile *Hemiaulus* aggregates throughout the sampled area at ~10 L^{-1}. Aggregated *Hemiaulus* represented the entire observed population at times and had a widespread distribution independent of the SEP. Aggregate occurrence was not consistent with a density dependent formation mechanism and may represent a natural

PeerJ Preprints NOT PEER-REVIEWED

growth form in undisturbed conditions. The photosynthetic potential index (F_v:F_m) increased from ~0.4 to ~0.6 during both blooms indicating a physiologically robust phytoplankton community in the blooms. The diel pattern of F_v:F_m(nocturnal maximum; diurnal minimum) was consistent with macronutrient limitation throughout the mission with no evidence of Fe-limitation despite the presence of nitrogen fixing diatom-diazotroph assemblages. During the 5-month mission, *Honey Badger* covered ~5690 km (3070 nautical miles), acquired 9336 holograms, and reliably transmitted data onshore in near real-time. Software issues developed with the active fluorescence sensor that terminated measurements in early September. Although images were still useful at the end of the mission, fouling of the LISST-Holo optics was considerable, and appeared to be the most significant issue facing deployments of this duration.

PeerJ Preprints NOT PEER-REVIEWED

Summer diatom blooms in the eastern North Pacific gyre investigated with a long-endurance autonomous surface vehicle

Emily E. Anderson[1], Cara Wilson[2], Anthony H. Knap[3], Tracy A. Villareal[1]

[1] Department of Marine Science and Marine Science Institute, The University of Texas at Austin, Port Aransas, Texas, United States of America

[2] NOAA/NMFS, Environmental Research Division, Monterey, California, United States of America

[33]Geochemical and Environmental Research Group, Texas A&M University, College Station, Texas, United States of America

corresponding author:

Tracy Villareal[1]

Email address: tracyv@austin.utexas.edu

PeerJ Preprints NOT PEER-REVIEWED

Abstract

Satellite chlorophyll (chl) observations have repeatedly observed summertime phytoplankton blooms in the North Pacific subtropical gyre (NPSG), a region of open ocean that is far removed from any land-derived or Ekman upwelling nutrient sources. These blooms are dominated by N_2-fixing diatom-cyanobacteria associations of the diatom genera *Rhizosolenia* Brightwell and *Hemiaulus* Ehrenberg. Their nitrogen fixing endosymbiont, *Richelia intracellularis* J.A. Schmidt, is hypothesized to be critical to the development of blooms in this nitrogen limited region. However, due to the remote location and unpredictable duration of the summer blooms, prolonged *in situ* observations are rare outside of the Station ALOHA time-series off of Hawai'i. In summer, 2015, a proof-of–concept mission using the autonomous vehicle, *Honey Badger* (Wave Glider SV2), collected near-surface (<20m) observations in the NPSG using hydrographic, meteorological, optical, and imaging sensors designed to focus on phytoplankton abundance, distribution and physiology of this bloom-forming region. *Hemiaulus* and *Rhizosolenia* cell abundance was determined using digital holography for the entire June-November mission. *Honey Badger* was not able to reach the 30° N subtropical front region where most of the satellite chl blooms have been observed, but near-real time navigational control allowed it to transect two blooms near 25° N. The two taxa did not co-occur in large numbers, rather the blooms were dominated by either *Hemiaulus* or *Rhizosolenia*. The 2-4 August 2015 bloom was comprised of 96% *Hemiaulus* and the second bloom, 15-17 August 2015, was dominated by *Rhizosolenia* (75%). The holograms also imaged undisturbed, fragile *Hemiaulus* aggregates throughout the sampled area at ~10 L^{-1}. Aggregated *Hemiaulus* represented the entire observed population at times and had a widespread distribution independent of the SEP. Aggregate occurrence was not consistent with a density dependent formation mechanism and may represent a natural growth form in undisturbed conditions. The

PeerJ Preprints NOT PEER-REVIEWED

photosynthetic potential index (F_v:F_m) increased from ~0.4 to ~0.6 during both blooms indicating a physiologically robust phytoplankton community in the blooms. The diel pattern of F_v:F_m (nocturnal maximum; diurnal minimum) was consistent with macronutrient limitation throughout the mission with no evidence of Fe-limitation despite the presence of nitrogen fixing diatom-diazotroph assemblages. During the 5-month mission, *Honey Badger* covered ~5690 km (3070 nautical miles), acquired 9336 holograms, and reliably transmitted data onshore in near real-time. Software issues developed with the active fluorescence sensor that terminated measurements in early September. Although images were still useful at the end of the mission, fouling of the LISST-Holo optics was considerable, and appeared to be the most significant issue facing deployments of this duration.

PeerJ Preprints NOT PEER-REVIEWED

55

56 **Introduction**

57 Low-nutrient, low chlorophyll (LNLC) oceanic regimes with chlorophyll-a (chl)
58 concentrations <0.07 mg m^{-3} constitute approximately 60% of the world ocean (Guieu et al.
59 2014) and are home to a phytoplankton community highly adapted for survival at the ambient
60 nanomolar concentrations of inorganic NO_3^- and PO_4^{-2}. One of the important adaptations is
61 nitrogen-fixation (diazotrophy), a process by which dissolved N_2 is converted into ammonium
62 for incorporation into amino acids and proteins (Carpenter & Capone 2008). Dizaotrophy
63 requires abundant iron resources (Mills et al. 2004; Ratten et al. 2015) and is reduced in iron-
64 limited regions. N_2-fixation may also be limited by other nutrients (Kustka et al. 2002; Mills et
65 al. 2004; Ratten et al. 2015) or competition by non-diazotrophic phytoplankton (Weber &
66 Deutsch 2014). Multiple prokaryote taxa are capable of diazotrophy (Zehr & Kudela 2011);
67 photosynthetic taxa include colonial cyanobacteria such as *Trichodesmium* spp. (Capone et al.
68 1997; Goering et al. 1966), free-living coccoid forms including *Crocosphaera watsonii* (Goebel
69 et al. 2008; Zehr et al. 2001), and coccoid or filamentous forms symbiotic with eukaryotes. Of
70 these latter symbioses, there are coccoid forms symbiotic with the prymnesiophyte
71 *Braarudosphaera bigelowii* (Gran and Braarud) Deflandre (Thompson et al. 2014; Thompson et
72 al. 2012), dinoflagellates (Farnelid et al. 2010; Foster et al. 2006) and filamentous or coccoid
73 cyanobacteria occurring as exo- or endosymbionts of diatoms (Foster & O'Mullan 2008;
74 Villareal 1992). This latter group, diatom-diazotroph associations (DDAs), are dominated by an
75 endosymbiosis between the filamentous cyanobacteria, *Richelia intracellularis*, and members of
76 the diatom genera *Rhizosolenia* and *Hemiaulus*. These symbioses have complex interactions with
77 their hosts (Foster & Zehr 2006; Hilton et al. 2013) and the taxonomic distinctness of the

PeerJ Preprints NOT PEER-REVIEWED

78 symbionts even within a single host genus remains unclear. DDAs play important roles in
79 biogeochemical cycling off the Amazon (Carpenter et al. 1999; Subramaniam et al. 2008) and
80 Mekong Rivers (Bombar et al. 2011) as well as in the central North Pacific gyre (Church et al.
81 2008).

82 At the Hawai'i Ocean Time-series (HOT), episodic pulses of DDAs dominated by
83 *Hemiaulus* spp. rapidly sink to depth (Scharek et al. 1999a; Scharek et al. 1999b) and transport
84 ~20% of the annual benthic carbon flux in a limited window (15 July-15 August) termed the
85 summer export pulse (SEP) (Karl et al. 2012). Isotopic signatures of N_2 fixation suggest that
86 their diazotrophic symbiont is present and fueling the biomass flux; the rapid sinking rate
87 indicates aggregation plays a key role in the accelerated transport to depth (Scharek et al. 1999b).
88 The SEP is possibly linked to episodic surface blooms of DDAs advecting through the region in
89 the prevailing flow (Dore et al. 2008; Fong et al. 2008; White et al. 2007). Auxospore formation
90 has also been offered as an explanation (Karl et al. 2012) although direct examination of trap
91 material (Scharek et al. 1999a; Scharek et al. 1999b) reported no evidence of auxosporulation.
92 Follett et al. (2018) modelled generalized DDA dynamics, noting that the population peaked in
93 the early summer and rapidly declined during the SEP window after a transition from modelled
94 Fe to P limitation favored competitive exclusion by other taxa. The model necessarily addressed
95 generalized conditions and did not address the localized blooms noted by satellites. These
96 blooms dominate in the summer (Wilson 2003) and are often associated with the unique
97 properties of mesoscale eddy flow-fields (Calil et al. 2011; Calil & Richards 2010; Guidi et al.
98 2012). There are few long-term, high frequency direct observations on DDA abundance to
99 evaluate these hypotheses.

PeerJ Preprints NOT PEER-REVIEWED

In the N. Pacific, the DDA host genus *Hemiaulus* is a characteristic upper euphotic zone species typically found across the central North Pacific gyre at levels of 10^2 cells L^{-1} (Venrick 1988; Venrick 1999). Near-surface blooms of both *Rhizosolenia* and *Hemiaulus* DDAs at 10^4+ cells L^{-1} (Venrick 1974) extend well north of Hawai'i at abundance up to 10^4 L^{-1} (Brzezinski et al. 1998; Krause et al. 2012; Villareal et al. 2011) and are frequently associated with summer chl blooms observed in satellite ocean color sensors (Villareal et al. 2011). These chl blooms (operationally defined as > 0.15 mg chl m^{-3}) north of 25.5° N cover a much greater range of temperatures and surface area than the blooms at HOT (~22.5° N) and extend at least as far north as 35.5° N (Villareal et al. 2012). While the data suggest that these satellite-observed blooms are probably associated with DDA events, it has remained difficult to sample these more northerly blooms due to the remote location, episodic timing and extensive geographic range. The applicability of the SEP to these areas is unclear, as is the general role of aggregation in *Hemiaulus* spp. biology. *In situ* diver observations suggest aggregation commonly occurs in *Hemiaulus* (Villareal et al. 2011), providing a means for rapid sinking as the bloom senesces. It is unclear whether *Hemiaulus* aggregation occurs as a density dependent process as noted in coastal diatom blooms (Burd & Jackson 2009; Jackson 2005), is a natural growth form of the genus similar to *Rhizosolenia* mats, is uniquely localized to the summer export window, or is a more generalized feature throughout the year. With recent observations of the ubiquitous presence of living diatom cells in the 2,000-4,000 depth strata, the role of aggregation in oceanic diatom biology has assumed new importance (Agusti et al. 2015).

Sampling these blooms outside of HOT is a challenge due to both the distance to blooms, unpredictable occurrence, long planning lead time, and cost involved in multiple week research

PeerJ Preprints NOT PEER-REVIEWED

cruises. Even at HOT, shipboard sampling is at approximately monthly intervals and insufficient to resolve episodic events in annual cycles. To address this, we used an SV2 Wave Glider (*Honey Badger*), a long-range autonomous vehicle utilizing wave power for propulsion and solar panel arrays on a surface float to provide power for a variety of sampling instruments (Daniel et al. 2011). While many types of autonomous vehicles are used in the marine environment (Dickey et al. 2008; Lee et al. 2017), the Wave Glider is particularly capable of multiple-month missions carrying extensive payloads, is under near-real time control, and has successfully transited from Hawai'i to Australia while returning oceanographic data (Villareal & Wilson 2014). They have been successfully deployed for sediment transport studies (Van Lancker & Baeye 2015), wind/current assessments of typhoons (Van Lancker & Baeye 2015), buoy validation exercises (Fitzpatrick et al. 2015), examination of air-sea coupling in the Southern Ocean (Thomson & Girton 2017), and processes controlling North Atlantic and Eastern Pacific Ocean salinity variability (Lindstrom et al. 2017).

In our study, we equipped the Wave Glider *Honey Badger* with a novel array of imaging and physiological sensors specifically targeting phytoplankton dynamics. We present data gathered during a 5-month mission in 2015 which sampled two diatom blooms. The mission objectives were to return the glider safely, determine if a holographic imaging system could quantify diatom events, relate the abundance to satellite observed chl blooms, examine the data for *Hemiaulus* aggregations, and acquire physiological data using active fluorescence.

Materials and Methods

The mission area for the *Honey Badger* was the eastern North Pacific subtropical gyre (NPSG) spanning 19-30° N and 144-157° W in the open waters northeast of the Hawaiian

PeerJ Preprints NOT PEER-REVIEWED

Islands (Fig. 1) where chl blooms regularly occur between July and October (Wilson 2003). Waypoints were chosen based on Aqua-MODIS 8-day composite chl concentration satellite images from the Environmental Research Division's ERDDAP (https://coastwatch.pfeg.noaa.gov/erddap/griddap/erdMBchla8day.html). After a preliminary deployment in the test area off Kawaihae, Hawai'i, the *Honey Badger* headed north on 1 June 2015. It was recovered on 3 November 2015 and returned to the test facility for evaluation and data download.

The Wave Glider® SV2 (Liquid Robotics, a Boeing company, Sunnyvale, CA) is an autonomous surface vehicle capable of extended operations offshore. It has a surface float (2.1 m x 0.6 m) connected by a 7 m umbilical to a subsurface glider (0.4 m x 1.9 m) with articulating wings (1.1 m wide) that uses vertical motion from waves to provide forward movement. Within the surface float, equipment bays provide space for computers, communications equipment and battery arrays powered by solar panels. Iridium satellite communication with the Wave Glider *Honey Badger* used in this mission was in near-real time and provided a near immediate ability to course correct and respond to environmental conditions.

The *Honey Badger* was equipped with sensors on the float, the sub-body, and on a towed body (Fig. 2; Table 1) The float contained 2 Turner Designs C3 fluorometers (Sunnyvale, CA) rimmed with anti-fouling copper, a Seabird Electronics gpCTD (Bellevue, WA) for water temperature and salinity with an inline antifouling tablet, a Canon G10 camera (Canon, USA Inc, Melville, NY) looking down through the float, a Datawell MOSE weather sensor (Datawell BV, Haarlem, The Netherlands), Airmar WX and WS weather sensors+light bar (Airmar Technology Corporation, Milford, NH), an AIS (automatic identification system) transponder and a radar reflector. The sub-body located 7 m below the float had an externally mounted Turner Designs

PeerJ Preprints NOT PEER-REVIEWED

PhytoFlash (Sunnyvale, CA) utilizing the data and power connections through the umbilical. The PhytoFlash sensor was shielded by a dark cap painted inside and out with anti-fouling paint. A Sequoia Scientific, Inc. (Bellevue, WA) Laser *In Situ* Scattering and Transmissometry Holographic System (LISST-Holo, termed Holo) was deployed in a neutrally buoyant towed body behind the *Honey Badger* on a 10 m tether equipped with scoops to passively direct water into the sample field. The tow fish varied from 6.3-15.5 m deep based on the Holo's internal depth sensor. The Holo drew power from the umbilical with the data stored in the Holo's onboard internal memory module. Bandwidth limitations did not permit transmission to shore via Iridium satellite. The Holo sample chamber was painted with antifouling paint and lined with copper tape on other surfaces to minimize fouling. Power consumption and available solar charging dictated sampling frequency and varied with the sensors (Table 1). The vehicle reported location and condition telemetry every 30 seconds. Sensors were integrated into the onboard processing and communications equipment by Liquid Robotics with the exception of the PhytoFlash. Software integration for the PhytoFlash and tow body construction was provided by the Geophysical Engineering Research Group (GERG) at Texas A&M University.

The Turner C3 fluorometers were equipped with filters for chl, phycoerythrin and colored dissolved organic material (CDOM) with values reported in fluorescence units. The C3 sensors were deployed on either side of the centerline with a port and starboard sensor. The port C3 sensor and optical port for the look-down camera were coated with a ~30 µm layer of ClearSignal antifouling compound (Severn Marine Technologies, Annapolis, MD) in spring, 2014. Due to technical difficulties, the mission was delayed a year with unknown effects on the viability of the coating. The look-down camera began recording on 1 July 2015 and imaged

PeerJ Preprints NOT PEER-REVIEWED

vertically below the float for examining the umbilical and glider as needed but also captured images of fish and biofouling over the course of the mission.

The Holo uses collimated laser light to create refraction patterns from particles that are then recorded by camera to create a hologram (Davies et al. 2015). Software provided by Sequoia Scientific Inc. (Holo_Batch v. 3.1) reconstructed multiple holograms into greyscale images. Particle biovolume was calculated based on a cross-section area projected into a sphere. Holo_Detail (v. 3.1) was used to process each hologram in greater detail to identify *Hemiaulus* and *Rhizosolenia* spp. Isolated hologram areas could be imaged individually as 0.1-1 mm thick sections allowing detailed images layer by layer. The sampling rate of 15 holographic images (30 s between images) every 6 hours was set prior to launch based on worst case power consumption calculations and could not be modified once underway. The 15-image bursts taken every 6 hours were combined to form one record yielding 4 records (bursts) d^{-1}. The Holo sampling volume was 1.86 ml per image with the 15-image burst sampling a total of 27.9 ml. Dye studies prior to the mission indicated the 30 second between images was sufficient for full chamber volume replacement.

The large file size (~2 MB) of each raw Holo hologram precluded satellite transmission and were only available for analysis after the *Honey Badger*'s recovery in November 2015. Upon recovery of the drive, 9336 holographic images were analyzed with the Holo_Batch and Holo_Detail at the University of Texas at Austin's Marine Science Institute. Comparison of Holo_Batch processing and individual Holo_Detail processing of the same images indicated progressive loss of recognizable diatoms over the mission due to biofouling (examples given in Fig. S1). Therefore, *Hemiaulus* and *Rhizosolenia* cells were quantified using the Holo_Detail software on every hologram with distinctive diffraction patterns indicating when particles were

present. While using the Holo_Detail to enumerate diatoms was more time-intensive than using the montages of in-focus particles produced by the Holo_Batch, it was necessary as the montages often failed to show *Hemiaulus* or *Rhizosolenia* cells when they were clearly identifiable in Holo_Detail. The small size of individual *Hemiaulus* cells (~15 µm) and light silicification also contributed to difficulties in using the batch analysis mode as biofouling interference increased.

The Holo's sampling capability allowed counting cells with a minimum concentration of 36 cells L^{-1}. Individual *Hemiaulus* cells were at the size threshold of the Holo and hard to differentiate from other small cells unless they were in recognizable chains. In addition, *Hemiaulus* cells occurred as both individual chains and aggregations of various size. Chains were defined as 3 or more *Hemiaulus* cells which formed a curve with clear ends which did not cross itself or others more than once. Aggregates were defined as *Hemiaulus* cells in a chain or multiple chains with multiple ends or no discernable ends which crossed itself, other chains, or other particles multiple times.

Hologram processing also returned calculated biovolume for all detected particles after calculating their equivalent spherical diameter. The biovolume was automatically separated into bins based on equivalent spherical diameter from 2.5 µm – 9847 µm (50 bins with the upper size limit of each bin being 1.18 times the lower limit). The diatoms of interest in this study have an equivalent spherical diameter between 13-60 µm so a subset of bins (13.1-58.1 µm) were chosen to focus the analysis. Holograms with schlieren (optical anomalies in transparent mediums), microbubbles or blank images were manually removed from the analyses.

Biofouling interference was removed using the manufacturer's recommended procedure to average the biovolume over large groups of images. This procedure generated a constant signal that represented a consistent particle presence assumed to be biofouling. We arbitrarily

PeerJ Preprints NOT PEER-REVIEWED

averaged groups of 510 holograms representing an 8.5-day window for a total of 14 background signatures. This signature was subtracted from each hologram in the specified window to generate a biofouling-corrected biovolume. Details of this correction and effects on the result are included as Supplemental Text and Fig. S1-S2.

Pulse Amplitude Modulation fluorometry (Schreiber 2004) determination of F_v:F_m (PhytoFlash sample frequency=6 samples hr^{-1}) was used to evaluate phytoplankton physiological health. The PhytoFlash sampled at 10 minute intervals but was accelerated to 1 minute intervals from 27-28 July to test the system's resiliency to increased sampling rates. The port C3 sensor was on a fixed 10 min sampling interval with 10 samples averaged to generate a single value. The starboard sensor was reprogrammable via remote communications and was varied in sampling timing and averaging at various points in the mission. Changes from multi-point averaging to single point reporting resulted in systematic and predictable baseline shifts. The reasons for these changes are unknown. Iron stress was evaluated using the variable fluorescence criteria of Behrenfeld and Milligan (2013) simplified for the lower sampling rate of the PhytoFlash. In a macronutrient limited environment with sufficient iron, the nocturnal F_v:F_m is greater than the diurnal F_v:F_m. In an iron limited environment, the reverse is true. Time averaging (nighttime average of 36 data points; 0800-1359 UTC and daytime average of 54 data points; 1800-0259 UTC) was required to obtain a stable signal and timed to avoid the observed crepuscular F_v:F_m excursions. The PhytoFlash shutdown and missed samples at an increasing frequency during the mission and eventually failed completely in early September (traced to software issues). To ensure a comparable day/night sampling, only periods with 75% or more of the expected number of samples were included in the iron-limitation analysis and both periods for a date were required to meet the above standard. These criteria resulted in the removal of 33

of the 94 days of data collected over the mission. The entire F_v:F_m dataset was plotted versus time for a visual inspection of the data as well.

Aqua MODIS satellite's 8-day composite of daily chl was used to produce an animation showing the development of the blooms in the NPSG during the 2015 bloom season (June-November) and the position of the *Honey Badger*'s track (Video S1 at https://figshare.com/articles/S1_movie_mp4/5993644). The raw data from the C3s, gpCTD, AIS, MOSE, PhytoFlash, and weather station are archived at both the NOAA ERDDAP site (http://coastwatch.pfeg.noaa.gov/erddap/search/index.html?page=1&itemsPerPage=1000&searchFor=liquidr) and BCO-DMO (http://www.bco-dmo.org/project/505589). The BCO-DMO site also contains the raw holograms, the biovolume data, as well as the *Hemiaulus* and *Rhizosolenia* abundance data.

Results

Extensive biofouling on several of the optical windows occurred during the mission. A time series of images from the look down camera illustrates the development over time of barnacles and associated organisms (Fig. S3). A metal incompatibility with internal screw in the LISST-Holo camera system mount resulted in significant corrosion (Fig. S4); however, it did not encroach into the sample plan and no data was lost. *Honey Badger* collected 5 months of salinity, surface water temperature, diatom abundance, photosynthetic activity, and biovolume data from the NPSG. A nine-point running average (Fig. 3, grey line) and daily average were used to remove changes due to rain events or sensor errors in the gpCTD. The daily averaged water salinity and temperature data (Fig. 3, color-coded by latitude) ranged from 22.8 to 27.8°C, and 34.6 to 35.6 salinity. The lower salinity water near Hawai'i is evident at the beginning and

PeerJ Preprints NOT PEER-REVIEWED

ending of the mission. The *Honey Badger* did not cross the sub-tropical front, which is characterized by salinity ~34.5 found at ~30° N (Wilson et al. 2013). The pronounced temperature-salinity gradient from the center of the gyre to Hawai'i is evident in the continuous decrease in salinity and increase in temperature along the straight line transect from the farthest north point (29.245° N 152.40° W) on 12 Sept. 2015 to just north of Hawai'i on 23 Oct. 2015 (20.67° N 155.47° W).

The study area underwent a general chl increase over the course of the mission that was evident visually as a shift from deep blue to light green in mid-July (Video S1). This increase was quantitatively expressed as the average of chl values from all pixels in the study area (Fig. 4). Following a period of uniformly low chl concentration throughout the study area in June-July 2015 (Fig. 4), in mid-July chl levels throughout the study area increased concurrent with increased chl variability (increased standard deviation around the mean) due to chl blooms (Video S1). This period of elevated bloom activity extended from 1 Aug to 15 Sept. During this period, there were multiple blooms evident where the satellite chl exceeded 0.2 mg m^{-3}. The brief decrease in late September was followed by an increase in average chl through the end of the mission.

The two float-mounted Turner C3 fluorometers produced erratic signals and random shifts in baseline values (Fig. 5). The sensors did not parallel each other except for a general increase in the cyanobacteria pigment phycoerythrin from ~21 Sept. 2015 to the end of the mission, nor did the satellite chlorophyll values at *Honey Badgers* location note similar fluctuations. The C3 data sets were excluded from further analysis due to a lack of an independent diagnostic test to determine which data points were reflective of the water properties and which were noise or errors introduced by the sensor.

PeerJ Preprints NOT PEER-REVIEWED

Hemiaulus and *Rhizosolenia* cells were readily identifiable in the processed holograms both as chains and aggregates (Fig. 6). *Hemiaulus* cells were identifiable as either curved or spiral chains (Fig. 6a) as well as aggregates of varying degrees of complexity (Fig. 6b, c). With three cells required to define identify a *Hemiaulus*, the minimum reported concentration is 108 cells L^{-1}. In *Rhizosolenia*, the symbiont of *Richelia intracelluaris* was visible as well (Fig. 6d arrows). Mean *Hemiaulus* abundance over the entire mission was 303 cells L^{-1} (s.d. = 1.0×10^3 cells L^{-1}, n = 610) and mean *Rhizosolenia* abundance was 63 cells L^{-1} (s.d. = 2.7×10^2 cells L^{-1}, n = 610) over all the samples. However, of the 610 samples, only 208 contained *Hemiaulus* cells and 207 contained *Rhizosolenia* cells. When present, the average *Hemiaulus* abundance was 8.9 $\times 10^2$ L^{-1} (s.d. = 1.6×10^3 cells L^{-1}, n = 208). Of the samples containing *Rhizosolenia* cells, the average abundance was 1.8 x 10^2 cells L^{-1} (s.d. = 4.5×10^2 cells L^{-1}, n = 207). *Hemiaulus* maximum abundance in the averaged 15 image burst was 1.4×10^4 cells L^{-1} on 2 August 2015 and the *Rhizosolenia* maximum abundance was 2.8×10^3 cells L^{-1} on 16 August 2015 (Fig. 7). Blooms were defined operationally as occurring when the abundance value was two s.d. above the mean present values, resulting in a threshold of 4×10^3 cells L^{-1} for *Hemiaulus* and 1×10^3 cells L^{-1} for *Rhizosolenia.*

Surface chlorophyll (satellite derived) at *Honey Badger's* position underwent a ~2 fold variation over the mission (Fig. 7a) with a sharp increase on 2 Aug. 2015, followed by considerable day to day patchiness evident throughout the rest of the mission. A similar pattern was seen in the Phytoflash F_m data from sub body at ~7 m (Fig. 7b) until the data collection failed on 1 Sept 2015. Two blooms were sampled, a *Hemiaulus* bloom on 2-4 August 2015 and a

PeerJ Preprints NOT PEER-REVIEWED

326 *Rhizosolenia* bloom on 15-17 August 2015. Diatom abundance (Fig. 7c, d) was patchy with two
327 order of magnitude changes occurring within between adjacent Holo bursts in the blooms, a
328 distance of approximately 10 km. The *Hemiaulus* bloom was dominated by *Hemiaulus* (96% of
329 total diatoms; Fig. 7c) while the *Rhizosolenia* bloom was dominated by *Rhizosolenia* (75% of
330 total diatoms; Fig. 7d). However, neither bloom reached the 0.15 mg m^{-3} chlorophyll threshold
331 used to identify a satellite chlorophyll bloom. The two blooms were separated in space and in
332 time (Fig. 7, 8) and both had increases in biovolume (Fig. 7e). The larger *Rhizosolenia* cells
333 contributed nearly 2/3 more biovolume on 15-17 August 2015 despite the cell numbers being
334 only 1/3 that of the *Hemiaulus* bloom. The satellite chl signature was still faint when *Honey*
335 *Badger* sampled the *Hemiaulus* bloom from 2-4 August 2015 (compare 8a and 8b) but continued
336 to develop after the *Honey Badger* left the area (Video S1). The *Rhizosolenia* bloom sampled by
337 the *Honey Badger* from 15-17 Aug 2015 did not have a well-defined satellite chl signal (Fig.
338 7a,c; 8b). However, the PhytoFlash F_m (Fig. 7f) was approximately 33% higher in the
339 *Rhizosolenia* bloom than the *Hemiaulus* bloom.

340 Two declining blooms evident in the chl animation were sampled (8/23-25/2015 and
341 9/14-16/2015; Video S1). In both cases, no aggregates were seen in the Holo and the maximum
342 local abundance ~300 cells L^{-1} was reached in only one burst in each area. The rest of the bursts
343 were devoid of *Hemiaulus*. However, the lookdown camera imaged what appeared to be a mass
344 occurrence of small white flocs (Fig. S3b). Their identity could not be confirmed, but the size
345 and shape are consistent with either marine aggregates or possibly colonial radiolarians.

346 Maximum F_v:F_m values (~0.6) were associated with the *Hemiaulus* and the *Rhizosolenia*
347 peak abundance values (Fig. 7e) although the data loss on 2 Aug. may have missed higher F_v:F_m

values. During the period of the two blooms (2-17 Aug), the F_v:F_m values underwent day to day changes in magnitude that were visibly distinct from the period before and after.

The Holo captured 31 *Hemiaulus* aggregates in 23 sampling bursts (Table 2 and 8c,d) out of 610 total bursts over the mission (3.8%) or 11% of samples when any *Hemiaulus* were present. Aggregates shared common characteristics of curled chains of various sizes tangled together to create a characteristic shape (Fig. 6) and were easily identified when compared to diver-collected aggregates (Fig. S5). When present, 72±25% (std. dev.) of the total *Hemiaulus* cells were present in aggregated form (Fig. 8c, Table 2). They were not limited to regions where non-aggregated *Hemiaulus* cells were abundant (Fig. 8c, d) and were observed from 27 June 2015 and 25 October 2015 with 13 of the 24 locations outside the time window of the SEP (green shading in 8d). Within the holograms containing *Hemiaulus* aggregates, the average number of identifiable aggregated cells was 47 (s.d. = 42, n = 31) with a minimum of 7 (two small crossed chains) and a maximum of 220. Due to the complex 3-dimensional structures of some of the aggregates, it is likely that cell counts for aggregates are underestimates.

A single aggregate in a 15 image burst represents, on average, 36 aggregates L^{-1}. Maximum abundance was present during the *Hemiaulus* bloom (2-4 Aug. 2015) where normalized abundance was 108 aggregates L^{-1}. The highest sustained aggregate abundance was during the early August bloom when aggregates were observed in 6 of 9 successive days (Table 2). However, there was no significant relationship between aggregated and non-aggregated cell abundance (r^2=0.12, p=0.5;) overall in the data set. On 3 of the 23 bursts where aggregates were observed, they were the only form of *Hemiaulus* present.

The F_v:F_m values underwent diel excursions typical of high-light populations experiencing solar-induced photoinhibition and down-regulation of photosynthetic activity where

PeerJ Preprints NOT PEER-REVIEWED

yields were greatest in the dark period and lower during the daytime (Fig. 9a). Crepuscular excursions were evident in many, but not all diel rhythms. From visual inspection of the entire mission dataset, there was no reversal of the diel rhythm suggestive of Fe-stress. The quantitative diurnal:nocturnal F_v:F_m ratio remained positive indicative of a macro-nutrient limited environment (Fig. 9b) although there was a long-term downward slope. The near zero values after 1 September 2015 were the result of compromised PhytoFlash data as the F_o and F_m values simultaneously drifted upwards resulting in loss of F_v:F_m (details in Fig. S6). 31 Aug. 2015 was the last date with uncompromised data before the PhytoFlash completely shutdown on 9 September 2015.

Discussion

Honey Badger as a sampling platform

Honey Badger successfully returned from a 5 month mission with all sensors undamaged. All sensors reported data, although at varying frequency and reliability, throughout the mission with the exception of the PhytoFlash. As a prototype mission, it was successful at deploying and recovering optical and imaging sensors specific to phytoplankton research questions. Individual sensors suffered from degradation associated with either platform computer software issues (PhytoFlash) or environmental biofouling (C3s and the LISST-Holo).

Post-mission inspection by Turner Designs indicated the PhytoFlash operated properly when removed from the glider, suggesting the system interface with the *Honey Badger* had failed. The SV2 was the first production model of Wave Gliders. The customized software used to power and communicate with the PhytoFlash was not part of the original system's dedicated software and gradually created insurmountable conflicts that led eventually to a complete failure.

PeerJ Preprints NOT PEER-REVIEWED

The newer generation (SV3) has a more robust on-board computer interface more amenable to customization and this is not likely to be a future issue.

One of the goals of the mission was to sample regions with chl concentrations >0.15 mg m^{-3}. The waypoints for *Honey Badger* were partially chosen based on the Aqua MODIS's chl data. Daily images were often incomplete due to cloud cover as well as being outside the daily imaging path. The 8-day composite of the Aqua MODIS satellite data provided a more complete image of the regional chl concentrations, However, the 8 day images used for daily decision making on the glider's movements were based on data that may have been up to 4 days old. This delay resulted in a few missed sampling opportunities (Video S1) since chl maps of the region the data were incomplete as waypoints were determined. This was particularly evident in the August *Hemiaulus* bloom. The magnitude of the bloom was not evident in the satellite imagery until the *Honey Badger* was a week past it and nearly halfway to a developing bloom to the west.

Biological observations

During the June to November timeframe of this mission, *Hemiaulus* and *Rhizosolenia* were the dominant diatom genera observed by the Holo in the NPSG chlorophyll blooms, reaffiming Guillard and Kilham's (1977) characterization of these taxa as persistent diatom representatives of the oligotrophic open ocean flora. The Holo's resolution limit (~15 µm) could not image the smaller pennate diatoms such as *Mastogloia* that frequently co-dominate in these blooms. The *Hemiaulus* abundance (10^4 cells L^{-1}) noted in the 2-4 August 2015 bloom is consistent with previous reports of open Pacific Ocean blooms where *Mastogloia* is a co-dominant (Brzezinski et al. 1998; Scharek et al. 1999a; Venrick 1974; Villareal et al. 2012).

PeerJ Preprints NOT PEER-REVIEWED

Thus, it is probable that additional diatoms were present and contributing to the satellite chl signature.

The patchiness in the abundance of both the *Hemiaulus* and *Rhizosolenia* DDA was unexpected. Approximately 2/3 of the bursts contained neither of these taxa. In some cases, the next sampling burst (6 hours later, or approximately 10 km) would observe ~10^3-10^4 cells L^{-1}. Such variation has been noted before from discrete ship sampling stations (Fong et al. 2008; Venrick 1974; Villareal et al. 2012) but with little ability to sustain 6 hour sampling intervals for months. The most extreme gradients were associated with developing blooms suggesting that the factors driving blooms are highly localized and not represented by the average nutrient or hydrographic characteristics. Calil (2011) reported satellite chl features in this gyre developed rapidly at frontal interfaces between mesoscale features as the result of sub-mesoscale ageostrophic flows resulting in transient up and downwelling. This spatial development scale is consistent with the abundance increase noted in the two observed diatom blooms and warrants further investigation into the role that mesoscale frontal features play in the DDA dynamics. However, there are no mechanisms suggested to address the variability in the background concentrations (10^1-10^2 cell L^{-1}) of these taxa presumably adapted to uniformly oligotrophic conditions.

Unlike previous studies using settled water samples or nets, we were able to record and partition *Hemiaulus* into aggregated or unaggregated abundance. *Hemiaulus* aggregates (Villareal et al. 2011) occurred throughout the mission, even in regions of low non-aggregated *Hemiaulus* abundance (Fig. 7, 9). The presence of 1 or more aggregates usually dominated the total abundance (Table 2) and on 3 occasions represented the entire *Hemiaulus* biomass seen. Maximum abundance (108 aggregates L^{-1}) and highest sustained aggregate abundance were both

present during the *Hemiaulus* bloom (2-4 Aug. 2015) where aggregated *Hemiaulus* represented 29-56% of the total *Hemiaulus* present in the bursts.

With an aggregate occurrence in 11% of the samples containing *Hemiaulus*, we examine what principles of diatom aggregation are relevant in this environment. Jackson's general coagulation model for diatom aggregates (Jackson 1990a; Jackson 1990b) suggest senescence, elevated concentrations, and enhanced stickiness play a key role in aggregation formation. In our data, aggregate density was highest in the August bloom, consistent with this model. However, the long chains and elevated F_v:F_m suggests a rapidly growing *Hemiaulus* population and the continued increase in the bloom area chlorophyll after *Honey Badger* departed (Video S1) suggests that this bloom was sampled early in its development. The aggregated form dominated total abundance when present, and aggregates appeared largely monospecific, at least within the resolution limits of the Holo. In contrast, diatom aggregates in coastal waters scavenge other particles and can sweep the water clear as they sink (Alldredge & Gotschalk 1989; Alldredge & Gotschalk 1990; Alldredge & Silver 1988). We suggest that aggregated forms of *Hemiaulus* are not solely the result of high rates of collision and sticking between *Hemiaulus* cell. Much like *Rhizosolenia* mats (Villareal & Carpenter 1989), they may be a natural growth form of *Hemiaulus* that results from curled chains twisting back on themselves. Further collisions may play a role but appear unlikely in the low density conditions that generally prevailed in this study.

Combined diver and net collections in 2003 (Villareal et al. 2011) found high *Hemiaulus* abundance was coupled to an aggregation snowstorm (Fig. S5) and allows us to examine whether the Holo's aggregate abundance data is credible. Using net-collected abundance data from the 2003 bloom (maximum abundance: 2,500 cells L^{-3}) and our average cells per aggregates in this

study (47), we calculate a potential for ~50 aggregates L^{-1} for the 2003 *Hemiaulus* snowstorm. The aggregates visible to divers (cm-sized) are substantially larger than the aggregates observed by the Holo (mm-sized), so this is likely an overestimate of abundance in the 2003 snowstorm. However, the value is similar to the detection limit represented by 1 aggregate per 15 image Holo burst (36 aggregates L^{-1}) and suggests the Holo data are the correct order of magnitude. Combined with the high proportion of samples containing aggregates (11%), our limited sample volume (~28 ml), the broad aggregate distribution, and the lack of a satellite signature from the 2003 snowstorm (Villareal et al. 2011), we conclude that dense *Hemiaulus* aggregation events are more common than reported. Pilskaln et al (2005) reported marine snow aggregates on the order of 1-10 L^{-1} at 28-30° N along a transect from HI to CA suggesting that *Hemiaulus* aggregates are part of rich collection of macroscopic particles rarely sampled. The incidental observation from the lookdown camera in a fading bloom of what appeared to be large aggregates in a fading bloom were at too low a density to be sampled by the Holo, but sufficiently large to be visible to the camera (Fig. S3b). Multiple imaging technologies on the vehicle are clearly needed to further detail this type of event.

Regularly occurring *Hemiaulus* aggregates could be an important food source to organisms in the open ocean due to their high concentration of carbon and nitrogen. They could also play an important role in the global carbon cycle since aggregated forms, when physiologically stressed, tend to sink much faster than non-aggregated particles (Stemmann & Boss 2012) and can scavenge other suspended particles as they sink to depth (Alldredge & Silver 1988). Station ALOHA sediment trap data indicated that during the 13 year record, the SEP sinking flux resulted in ~ 20% of the annual carbon export to the benthos at >5,000 m (Karl et al. 2012) with high sinking rates (10^2 m d^{-1}) requiring aggregates as a dominant mode of transport

485 (Scharek et al. 1999a; Scharek et al. 1999b). Our data show that *Hemiaulus* aggregates extend
486 deep into the N. Pacific gyre and support the idea that the role of the SEP may be much wider
487 than Sta. ALOHA waters near Hawai'i. However, there is no evidence that aggregate formation,
488 per se, is linked to the hypothesized annual rhythm driving the SEP. They occur independently of
489 the SEP.

490 We found no evidence of iron limitation during our sampling with the caveat that the
491 PhytoFlash measures a bulk water property, not a DDA specific stress. However, even during the
492 *Hemiaulus* and *Rhizosolenia* blooms observed on 3 August 2015 and 16 August 2015, the Fe
493 index did not suggest iron limitation or iron stress. From 1 June 2015 to 31 Aug. 2015, the dark-
494 averaged F_v:F_m stayed above the light-averaged values, agreeing with the 2006 study by
495 Behrenfeld et al. (2006) which classified this area as having a type I regime with low
496 macronutrients but sufficient iron supplies.
497

498 **Conclusions**

499 The *Honey Badger* offered a unique look into the remote oligotrophic North Pacific
500 subtropical gyre during its 5 month, 5690 km mission. While some of the sensors failed during
501 the mission (PhytoFlash) or produced uninterpretable data (C3s), the mission was a success in
502 that other sensors (LISST-Holo) recorded novel data over an extensive period of time (5-months)
503 and wide geographic extent, and the glider returned intact. *The Honey Badger* and its sensors
504 allowed for a persistent presence in the NPSG during the late summer/early fall bloom season.

505 The long-term deployment of both imaging and physiological sensors on a mobile
506 sampling platform provided novel information on the composition and physiology of remote
507 diatom blooms. The region showed no evidence of iron limitation despite the presence of DDAs

at 10^4 concentrations. *Hemiaulus* aggregates were widespread and observed outside the 15 July – 15 August SEP (Karl et al. 2012) window suggesting that the predictable timing of the SEP cannot be uniquely attributed to a rhythm in aggregate formation. If aggregates are consistent vectors for vertical transport at some stage, then the potential for a basin-wide SEP is enhanced. When present, *Hemiaulus* aggregates are abundant ($10+ L^{-1}$) and dominate the total *Hemiaulus* present. Their general characteristics are distinct from coastal diatom aggregates and more similar to *Rhizosolenia* mats (Alldredge & Silver 1982; Carpenter et al. 1977; Villareal et al. 2014), suggesting *Hemiaulus* aggregates are a natural growth form. Their broad and persistent occurrence suggests they do not have consistently high sinking rates. The PhytoFlash and the Holo data are generally uncoupled from the satellite chl concentrations which illustrates the added value of *in situ* sampling to understand the community structure and physiological needs of these blooms in remote open ocean habitats.

Acknowledgements

We wish to thank Liquid Robotics, a Boeing company, for providing the glider time as part of the PacX Challenge award and our project manager Danny Merritt for his contributions to the mission success. We acknowledge John Walpert (GERG) for adapting some of equipment to the SV2. In addition, the skilled field testing and support provided by Brad Woolhiser, Chuck Shaver, Dustin Boettcher, and Vas Podorean at the LR test facility in Kawaihae, HI is gratefully acknowledged. We wish to thank Bob Simons (SWFSC/ERD) for putting the *Honey Badger* data on ERDDAP and Lynn DeWitt (SWFSC/ERD) for creating the project website (http://oceanview.pfeg.noaa.gov/MAGI).

PeerJ Preprints NOT PEER-REVIEWED

References

Agusti S, González-Gordillo JI, Vaqué D, Estrada M, Cerezo MI, Salazar G, Gasol JM, and Duarte CM. 2015. Ubiquitous healthy diatoms in the deep sea confirm deep carbon injection by the biological pump. *Nature Communications* 6:7608. 10.1038/ncomms8608

Alldredge AL, and Gotschalk CC. 1989. Direct observations of the mass flocculation of diatom blooms: characteristics, settling velocities and formation of diatom aggregates. *Deep-Sea Research* 36:159-171.

Alldredge AL, and Gotschalk CC. 1990. The relative contribution of marine snow of different origins to biological processes in coastal waters. 10:41-58.

Alldredge AL, and Silver MW. 1982. Abundance and production rates of floating diatom mats (*Rhizosolenia castracanei* and *Rhizosolenia imbricata* var. *shrubsolei*) in the eastern Pacific Ocean. *Marine Biology (Berlin)* 66:83-88.

Alldredge AL, and Silver MW. 1988. Characteristics, dynamics and significance of marine snow. *Progress in Oceanography* 20:41-82.

Behrenfeld M, Worthington K, Sherrell RM, Chavez FP, Strutton P, McPhaden M, and Shea DM. 2006. Controls on tropical Pacific Ocean productivity revealed through nutrient stress diagnostics. *Nature (London)* 442:1025-1028. DOI:10.1038

Behrenfeld MJ, and Milligan AJ. 2013. Photophysiological expressions of iron stress in phytoplankton. In: Carlson CA, and Giovannoni SJ, eds. *Annual Review of Marine Science, Vol 5*, 217-246.

Bombar D, Moisander PH, Dippner JW, Foster RA, Voss M, Karfeld B, and Zehr JP. 2011. Distribution of diazotrophic microorganisms and nifH gene expression in the Mekong River plume during intermonsoon. *Marine Ecology-Progress Series* 424:39-U55. 10.3354/meps08976

Brzezinski MA, Villareal TA, and Lipschultz F. 1998. Silica production and the contribution of diatoms to new and primary production in the central North Pacific. *Marine Ecology Progress Series* 167:89-101.

Burd AB, and Jackson GA. 2009. Particle Aggregation. *Annual Review of Marine Science* 1:65-90. 10.1146/annurev.marine.010908.163904

Calil PHR, Doney SC, Yumimoto K, Eguchi K, and Takemura T. 2011. Episodic upwelling and dust deposition as bloom triggers in low-nutrient, low-chlorophyll regions. *Journal of Geophysical Research-Oceans* 116:doi: C06030 06010.01029/02010jc006704. C06030 10.1029/2010jc006704

Calil PHR, and Richards KJ. 2010. Transient upwelling hot spots in the oligotrophic North Pacific. *Journal of Geophysical Research-Oceans* 115:DOI: 10.1029/2009jc005360. C02003 10.1029/2009jc005360

Capone DG, Zehr JP, Paerl HW, Bergman B, and Carpenter EJ. 1997. Trichodesmium, a globally significant marine cyanobacterium. *Science (Washington, DC)* 276:1221-1229. 10.1126/science.276.5316.1221

Carpenter EJ, and Capone DG. 2008. Nitrogen fixation in the marine environment. In: Capone DG, Bronk DA, Mulholland MR, and Carpenter EJ, eds. *Nitrogen in the Marine Environment*: Elsevier, 141-198.

Carpenter EJ, Harbison RG, Madin LP, Swanberg NR, Biggs DC, Hulburt EM, McAlister VL, and McCarthy JJ. 1977. *Rhizosolenia* Mats. *Limnology and Oceanography* 22:739-741.

PeerJ Preprints NOT PEER-REVIEWED

Carpenter EJ, Montoya JP, Burns J, Mulholland MR, Subramaniam A, and Capone DG. 1999. Extensive bloom of a N_2-fixing diatom/cyanobacterial association in the tropical Atlantic Ocean. *Marine Ecology-Progress Series* 185:273-283.

Church MJ, Bjorkman KM, Karl DM, Saito MA, and Zehr JP. 2008. Regional distributions of nitrogen-fixing bacteria in the Pacific Ocean. *Limnology and Oceanography* 53:63-77.

Daniel T, Manley J, and Trenaman N. 2011. The Wave Glider: enabling a new approach to persistent ocean observation and research. *Ocean Dynamics* 61:1509-1520. 10.1007/s10236-011-0408-5

Davies EJ, Buscombe D, Graham GW, and Nimmo-Smith WAM. 2015. Evaluating Unsupervised Methods to Size and Classify Suspended Particles Using Digital In-Line Holography. *Journal of Atmospheric and Oceanic Technology* 32:1241-1256. 10.1175/jtech-d-14-00157.1

Dickey TD, Itsweire EC, Moline MA, and Perry MJ. 2008. Introduction to the Limnology and Oceanography Special Issue on Autonomous and Lagrangian Platforms and Sensors (ALPS). *Limnology and Oceanography* 53:2057-2061. 10.4319/lo.2008.53.5_part_2.2057

Dore JE, Letelier RM, Church MJ, Lukas R, and Karl DM. 2008. Summer phytoplankton blooms in the oligotrophic North Pacific Subtropical Gyre: Historical perspective and recent observations. *Progress in Oceanography* 76:2-38.

Farnelid H, Tarangkoon W, Hansen G, Hansen PJ, and Riemann L. 2010. Putative N_2-fixing heterotrophic bacteria associated with dinoflagellate-cyanobacteria consortia in the low-nitrogen Indian Ocean. *Aquatic Microbial Ecology* 61:105-117. 10.3354/ame01440

Fitzpatrick PJ, Lau Y, Moorhead R, Skarke A, Merritt D, Kreider K, Brown C, Canon R, Hine G, Lampoudi T, and Leonardi AP. 2015. A Review of the 2014 Gulf of Mexico Wave Glider (R) Field Program. *Marine Technology Society Journal* 49:64-71. 10.4031/mtsj.49.3.14

Follett CL, Dutkiewicz S, Karl DM, Inomura K, and Follows MJ. 2018. Seasonal resource conditions favor a summertime increase in North Pacific diatom–diazotroph associations. *The ISME Journal*. 10.1038/s41396-017-0012-x

Fong AA, Karl DM, Lukas R, Letelier RM, Zehr JP, and Church MJ. 2008. Nitrogen fixation in an anticyclonic eddy in the oligotrophic North Pacific Ocean. *Isme Journal* 2:663-676. 10.1038/ismej.2008.22

Foster RA, Carpenter EJ, and Bergman B. 2006. Unicellular cyanobionts in open ocean dinoflagellates, radiolarians, and tintinnids: Ultrastructural characterization and immuno-localization of phycoerythrin and nitrogenase. *Journal of Phycology* 42:453-463.

Foster RA, and O'Mullan GD. 2008. Nitrogen-fixing and nitrifying symbioses in the marine environment. In: Capone DG, Bronk DA, Mulholland MR, and Carpenter EJ, eds. *Nitrogen in the Marine Environment, 2nd Edition*. San Diego: Elsevier, 1197-1218.

Foster RA, and Zehr JP. 2006. Characterization of diatom-cyanobacteria symbioses on the basis of nifH, hetR and 16S rRNA sequences. *Environmental Microbiology* 8:1913-1925. 10.1111/j.1462-2920.2006.01068.x

Goebel NL, Edwards CA, Carter BJ, Achilles KM, and Zehr JP. 2008. Growth and carbon content of three different-sized diazotrophic cyanobacteria observed in the subtropical North Pacific. *Journal of Phycology* 44:1212-1220. 10.1111/j.1529-8817.2008.00581.x

Goering JJ, Dugdale RC, and Menzel DW. 1966. Estimates of in situ rates of nitrogen uptake by *Trichodesmium* sp. in the tropical Atlantic Ocean. *Limnology and Oceanography* 11:614-620.

PeerJ Preprints NOT PEER-REVIEWED

Guidi L, Calil PHR, Duhamel S, Bjoerkman KM, Doney SC, Jackson GA, Li B, Church MJ, Tozzi S, Kolber ZS, Richards KJ, Fong AA, Letelier RM, Gorsky G, Stemmann L, and Karl DM. 2012. Does eddy-eddy interaction control surface phytoplankton distribution and carbon export in the North Pacific Subtropical Gyre? *Journal of Geophysical Research-Biogeosciences* 117. 10.1029/2012jg001984

Guieu C, Aumont O, Paytan A, Bopp L, Law CS, Mahowald N, Achterberg EP, Marañón E, Salihoglu B, Crise A, Wagener T, Herut B, Desboeufs K, Kanakidou M, Olgun N, Peters F, Pulido-Villena E, Tovar-Sanchez A, and Völker C. 2014. The significance of the episodic nature of atmospheric deposition to Low Nutrient Low Chlorophyll regions. *Global Biogeochemical Cycles* 28:1179-1198. 10.1002/2014GB004852

Guillard RRL, and Kilham P. 1977. The ecology of marine planktonic diatoms. In: Werner D, ed. *The Biology of Diatoms*. Berkeley: University of California Press, 372-346.

Hilton JA, Rachel AF, Tripp HJ, Brandon JC, Jonathan PZ, and Villareal TA. 2013. Genomic deletions disrupt nitrogen metabolism pathways of a cyanobacterial diatom symbiont. *Nature Communications* 4:1767-1767. 10.1038/ncomms2748

Jackson GA. 1990a. Limitation of algal blooms by formation of flocs through physical coagulation. *EOS* 71:185.

Jackson GA. 1990b. A model of the formation of marine algal flocs by physical coagulation processes. *Deep-Sea Research* 37:1197-1211.

Jackson GA. 2005. *Coagulation theory and models of oceanic plankton aggregation*. Boca Raton: Crc Press-Taylor & Francis Group.

Karl DM, Church MJ, Dore JE, Letelier RM, and Mahaffey C. 2012. Predictable and efficient carbon sequestration in the North Pacific Ocean supported by symbiotic nitrogen fixation. *Proceedings of the National Academy of Sciences* 109:1842-1849.

Krause JW, Brzezinski MA, Villareal TA, and Wilson C. 2012. Increased kinetic efficiency for silicic acid uptake as a driver of summer diatom blooms in the North Pacific gyre. *Limnology and Oceanography* 57:1084-1098. DOI: 10.4319/lo.2012.57.4.1084

Kustka A, Carpenter EJ, and Sanudo-Wilhelmy SA. 2002. Iron and marine nitrogen fixation: progress and future directions. *Research in Microbiology* 153:255-262.

Lee CM, Paluszkiewicz T, Rudnick DL, Omand MM, and Todd RE. 2017. Autonomous instruments significantly expand ocean observing An introduction to the special issue on autonomous and lagrangian platforms and sensors (ALPS). *Oceanography* 30:15-17. 10.5670/oceanog.2017.211

Lindstrom EJ, Shcherbina AY, Rainville L, Farrar JT, Centurioni LR, Dong SF, D'Asaro EA, Eriksen C, Fratantoni DM, Hodges BA, Hormann V, Kessler WS, Lee CM, Riser SC, St Laurent L, and Volkov DL. 2017. Autonomous multi-platform observations during the salinity processes in the upper-ocean regional study. *Oceanography* 30:38-48. 10.5670/oceanog.2017.218

Mills MM, Ridame C, Davey M, La Roche J, and Geider RJ. 2004. Iron and phosphorus co-limit nitrogen fixation in the eastern tropical North Atlantic. *Nature (London)* 429:292-294.

Pilskaln CH, Villareal TA, Dennett M, Darkangelo-Wood C, and Meadows G. 2005. High concentrations of marine snow and diatom algal mats in the North Pacific Subtropical Gyre: Implications for carbon and nitrogen cycles in the oligotrophic ocean. *Deep-Sea Research Part I-Oceanographic Research Papers* 52:2315-2332.

Ratten JM, LaRoche J, Desai DK, Shelley RU, Landing WM, Boyle E, Cutter GA, and Langlois RJ. 2015. Sources of iron and phosphate affect the distribution of diazotrophs in the

PeerJ Preprints NOT PEER-REVIEWED

North Atlantic. *Deep-Sea Research Part Ii-Topical Studies in Oceanography* 116:332-341. 10.1016/j.dsr2.2014.11.012

Scharek R, Latasa M, Karl DM, and Bidigare RR. 1999a. Temporal variations in diatom abundance and downward vertical flux in the oligotrophic North Pacific gyre. *Deep-Sea Research Part I-Oceanographic Research Papers* 46:1051-1075.

Scharek R, Tupas LM, and Karl DM. 1999b. Diatom fluxes to the deep sea in the oligotrophic North Pacific gyre at Station ALOHA. *Marine Ecology-Progress Series* 182:55-67.

Schreiber U. 2004. *Pulse-amplitude-modulation (PAM) fluorometry and saturation pulse method: An overview*.

Stemmann L, and Boss E. 2012. Plankton and particle size and packaging: from determining optical properties to driving the biological pump. In: Carlson CA, and Giovannoni SJ, eds. *Annual Review of Marine Science, Vol 4*, 263-290.

Subramaniam A, Yager PL, Carpenter EJ, Mahaffey C, Bjorkman K, Cooley S, Kustka AB, Montoya JP, Sanudo-Wilhelmy SA, Shipe R, and Capone DG. 2008. Amazon River enhances diazotrophy and carbon sequestration in the tropical North Atlantic Ocean. *Proceedings of the National Academy of Sciences of the United States of America* 105:10460-10465. 10.1073/pnas.0710279105

Thompson A, Carter BJ, Turk-Kubo K, Malfatti F, Azam F, and Zehr JP. 2014. Genetic diversity of the unicellular nitrogen-fixing cyanobacteria UCYN-A and its prymnesiophyte host. *Environmental Microbiology* 16:3238-3249. 10.1111/1462-2920.12490

Thompson AW, Foster RA, Krupke A, Carter BJ, Musat N, Vaulot D, Kuypers MMM, and Zehr JP. 2012. Unicellular cyanobacterium symbiotic with a single-celled eukaryotic alga. *Science (Washington, DC)* 337:1546-1550. 10.1126/science.1222700

Thomson J, and Girton J. 2017. Sustained Measurements of Southern Ocean Air-Sea Coupling from a Wave Glider Autonomous Surface Vehicle. *Oceanography* 30:104-109. 10.5670/oceanog.2017.228

Van Lancker V, and Baeye M. 2015. Wave glider monitoring of sediment transport and dredge plumes in a shallow marine sandbank environment. *PLoS ONE* 10:e0128948.

Venrick EL. 1974. The distribution and significance of *Richelia intracellularis* Schmidt in the North Pacific Central Gyre. *Limnology and Oceanography* 19:437-445.

Venrick EL. 1988. The vertical distributions of chlorophyll and phytoplankton species in the North Pacific central environment. *Journal of Plankton Research* 10:987-998.

Venrick EL. 1999. Phytoplankton species structure in the central North Pacific, 1973-1996: variability and persistence. *Journal of Plankton Research* 21:1029-1042.

Villareal TA. 1992. Marine nitrogen-fixing diatom-cyanobacterial symbioses. In: Carpenter EJ, Capone DG, and Reuter J, eds. *Marine Pelagic Cyanobacteria: Trichodesmium and other Diazotrophs*. Netherlands: Kluwer, 163-175.

Villareal TA, Adornato L, Wilson C, and Shoenbachler CA. 2011. Summer blooms of diatom-diazotroph assemblages (DDAs) and surface chlorophyll in the N. Pacific gyre – a disconnect. *Journal of Geophysical Research-Oceans* 116:DOI: 10.1029/2010JC006268. 10.1029/2010JC006268

Villareal TA, Brown CG, Brzezinski MA, Krause JW, and Wilson C. 2012. Summer diatom blooms in the North Pacific subtropical gyre: 2008-2009. *PLoS ONE* 7:e33109. doi:33110.31371/journal.pone.0033109.

PeerJ Preprints NOT PEER-REVIEWED

712 Villareal TA, and Carpenter EJ. 1989. Nitrogen-fixation, suspension characteristics and chemical
713 composition of *Rhizosolenia* mats in the central North Pacific Gyre. *Biological*
714 *Oceanography* 6:327-345.
715 Villareal TA, Pilskaln CH, Montoya JP, and Dennett M. 2014. Upward nitrate transport by
716 phytoplankton in oceanic waters: balancing nutrient budgets in oligotrophic seas. *PeerJ*
717 2:e302. 10.7717/peerj.302
718 Villareal TA, and Wilson C. 2014. A comparison of the Pac-X Trans-Pacific Wave glider data
719 and satellite data (MODIS, Aquarius, TRMM and VIIRS). *PLoS ONE* 9:e92280.
720 10.1371/journal.pone.0092280
721 Weber T, and Deutsch C. 2014. Local versus basin-scale limitation of marine nitrogen fixation.
722 *Proceedings of the National Academy of Sciences* 111:8741-8746.
723 10.1073/pnas.1317193111
724 White AE, Spitz YH, and Letelier RM. 2007. What factors are driving summer phytoplankton
725 blooms in the North Pacific Subtropical Gyre? *Journal of Geophysical Research-Oceans*
726 112. C12006 10.1029/2007jc004129
727 Wilson C. 2003. Late Summer chlorophyll blooms in the oligotrophic North Pacific Subtropical
728 Gyre. *Geophysical Research Letters* 30:1942, doi:1910.1029/2003GL017770.
729 Wilson C, Villareal TA, Brzezinski MA, Krause JW, and Shcherbina AY. 2013. Chlorophyll
730 bloom development and the subtropical front in the North Pacific. *Journal of*
731 *Geophysical Research: Oceans* 118:1-16. 10.1002/jgrc.20143
732 Zehr JP, and Kudela RM. 2011. Nitrogen Cycle of the Open Ocean: From Genes to Ecosystems.
733 In: Carlson CA, and Giovannoni SJ, eds. *Annual Review of Marine Science, Vol 3*, 197-
734 225.
735 Zehr JP, Waterbury JB, Turner PJ, Montoya JP, Omoregie E, Steward GF, Hansen A, and Karl
736 DM. 2001. Unicellular cyanobacteria fix N_2 in the subtropical North Pacific Ocean.
737 *Nature (London)* 412:635-638. 10.1038/35088063
738

PeerJ Preprints NOT PEER-REVIEWED

Figure 1

Mission track of the SV2 Wave Glider *Honey Badger*.

Mid-day positions points are color-coded by month. The asterisk north of Oahu is Station ALOHA of the Hawai'i Ocean Time-Series (HOT).

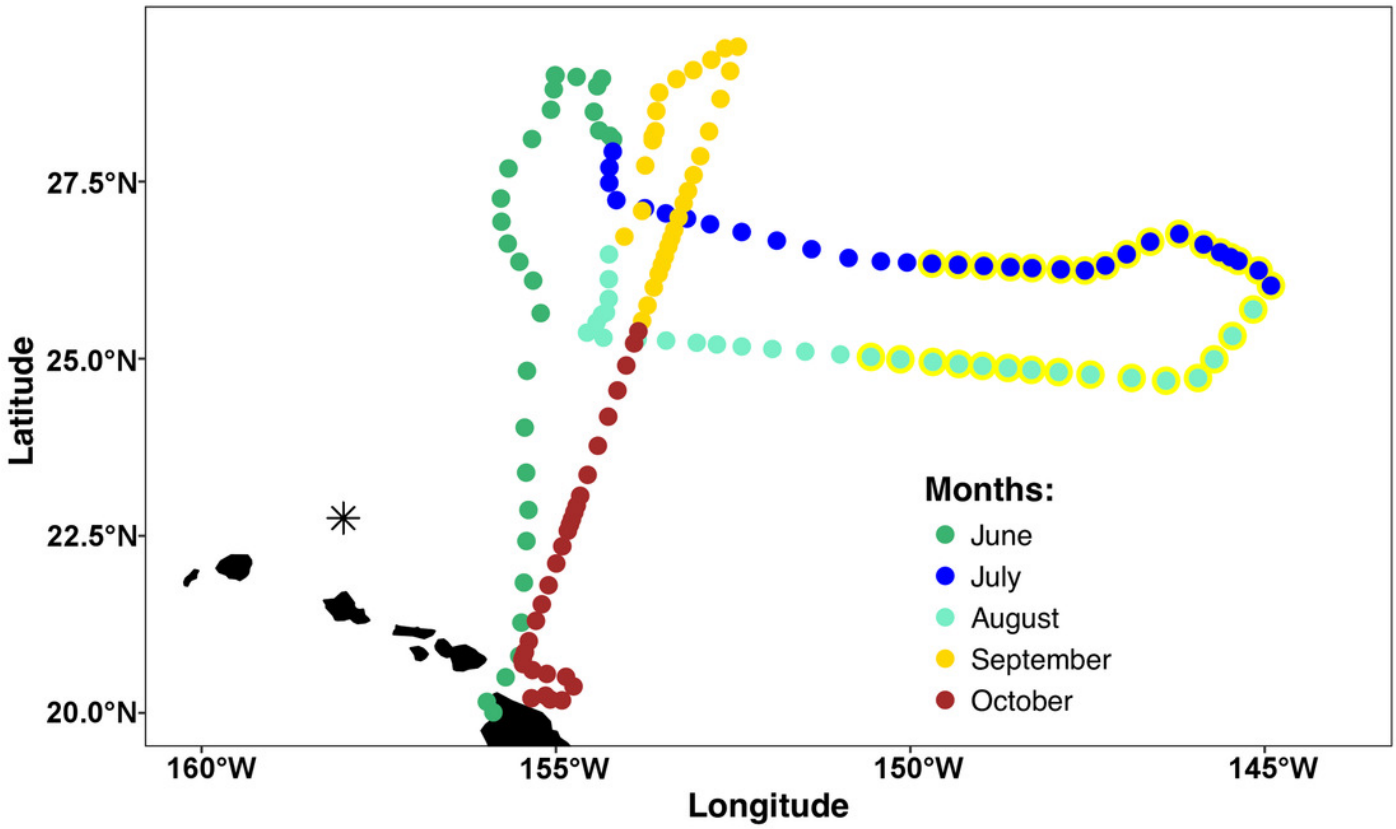

PeerJ Preprints NOT PEER-REVIEWED

Figure 2

Honey Badger diagram and sensor locations.

Schematic provided courtesy of Liquid Robotics, a Boeing Company.

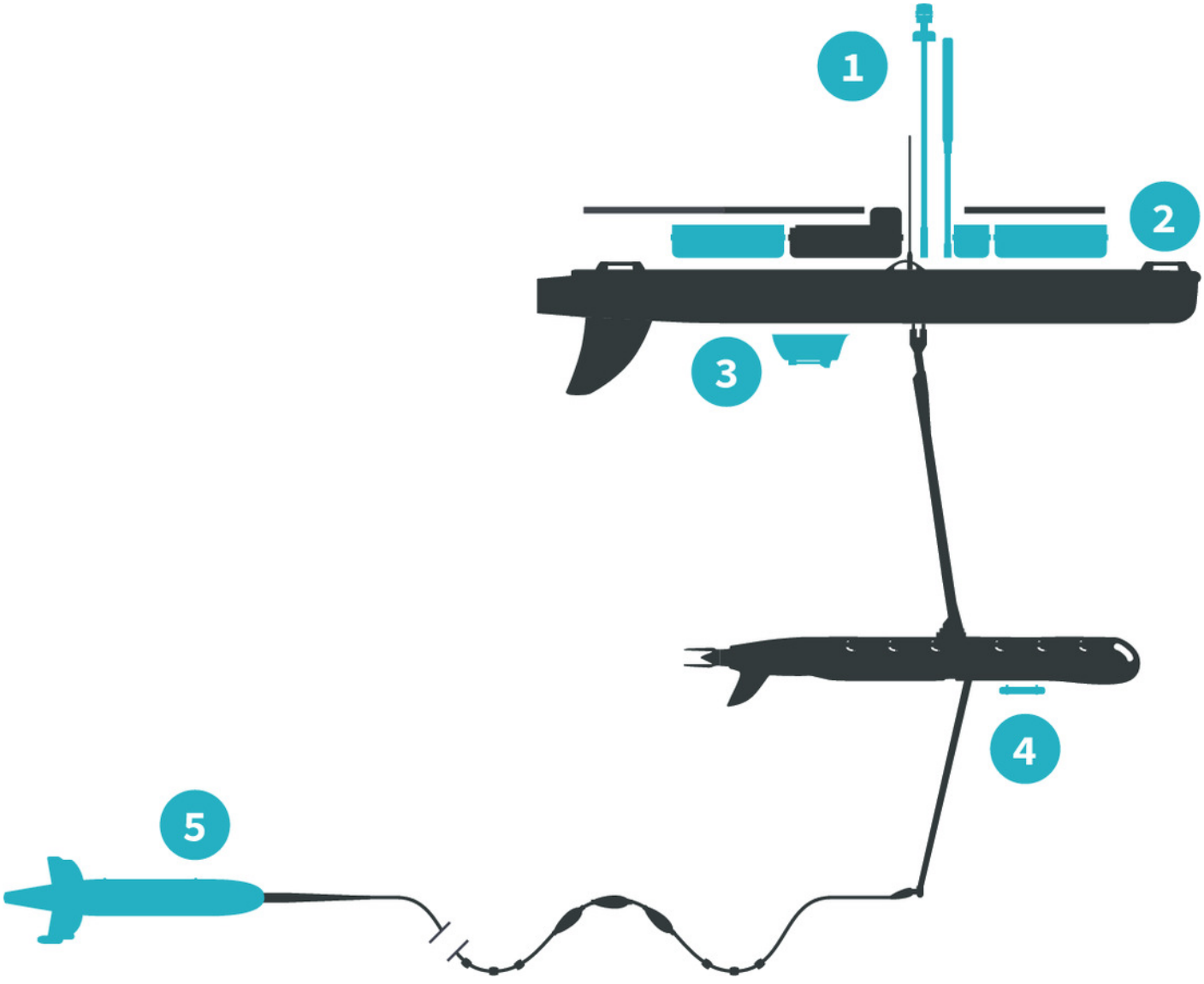

PeerJ Preprints | https://doi.org/10.7287/peerj.preprints.26961v1 | CC BY 4.0 Open Access | rec: 26 May 2018, publ: 26 May 2018

Figure 3

Time series of the hydrographic properties from the *Honey Badger*'s gpCTD sensor.

(A) Salinity (PSU). (B) Temperature (°C). The grey lines are the data with a 9-point smoothing, the color-coded dots are daily average values.

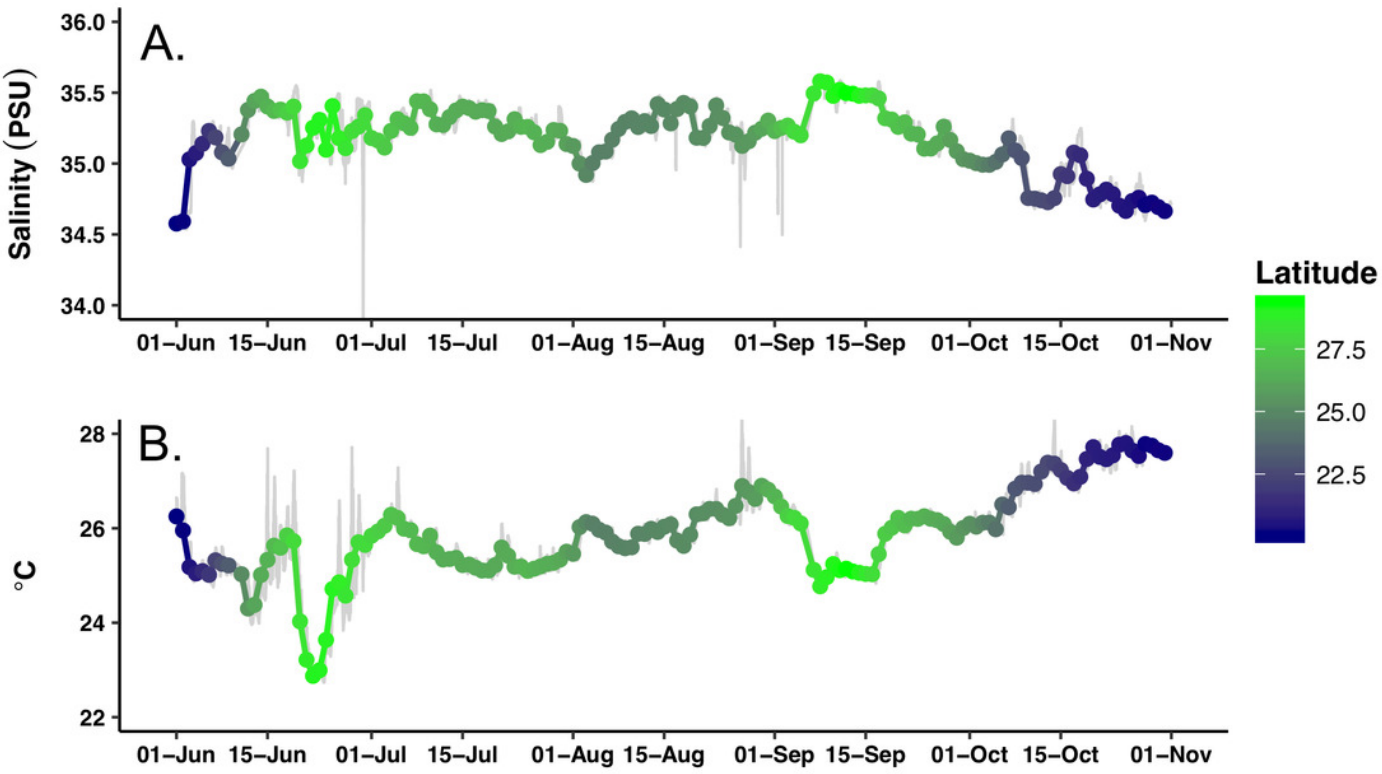

Figure 4

Average chl concentration of the study area over time.

All chlorophyll per pixel values from Aqua MODIS 8-day composite data within the study area (bounded by 19 to 30°N and 157-144°W) were averaged to generate a single daily value for the study area. Solid line = average chl concentration for the study area. Dashed lines = average chl concentration ± 1 standard deviation.v

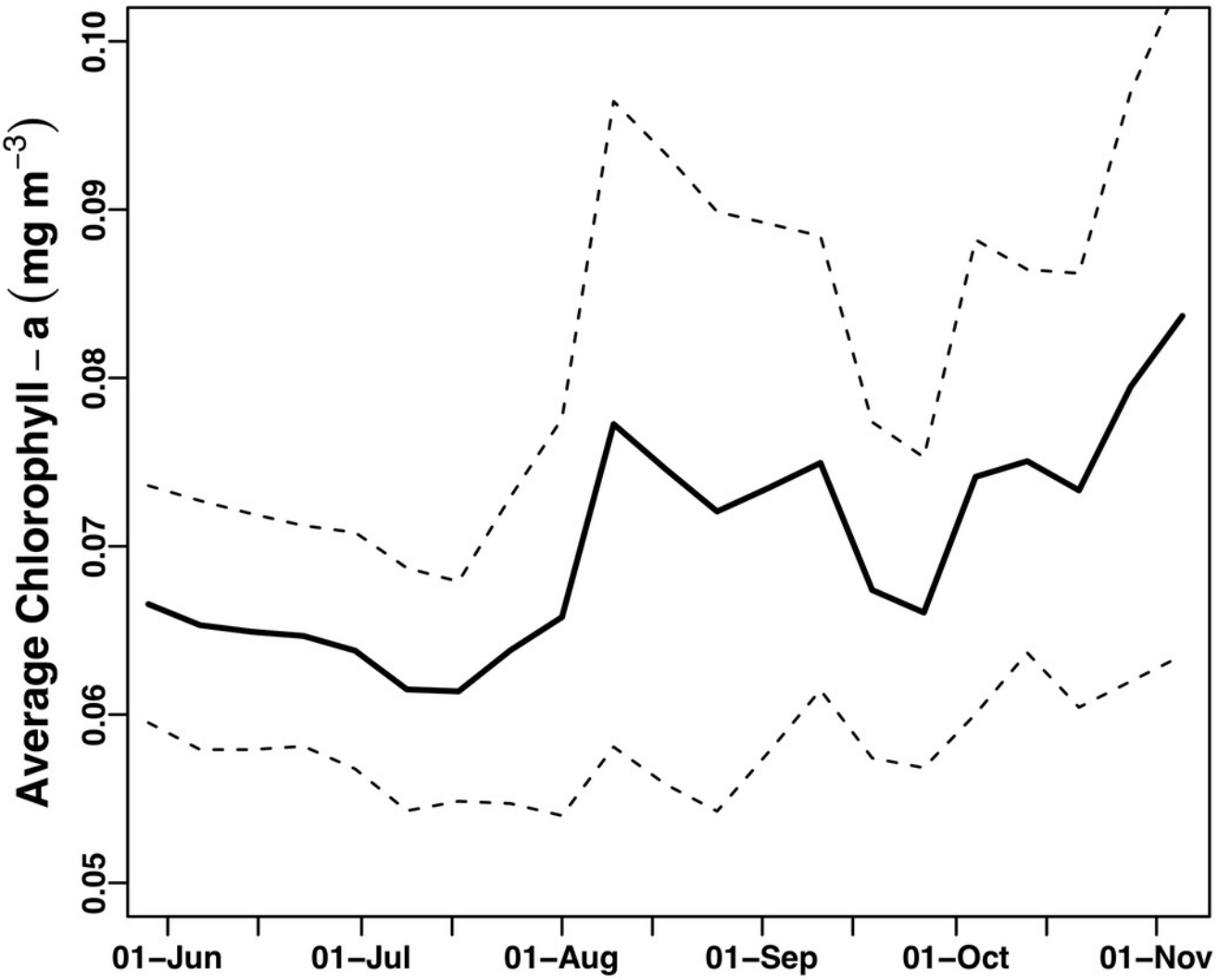

Figure 5

C3 fluorometer data from the *Honey Badger*.

Note scale shifts between plots. (A-C) Sensor coated with antifouling compound. (A) Chl. (B) CDOM. (C) Phycoerythrin. (D-F) uncoated sensor. (D) Chl. (E) CDOM. (F) Phycoerythrin. RFU = relative fluorescence units.

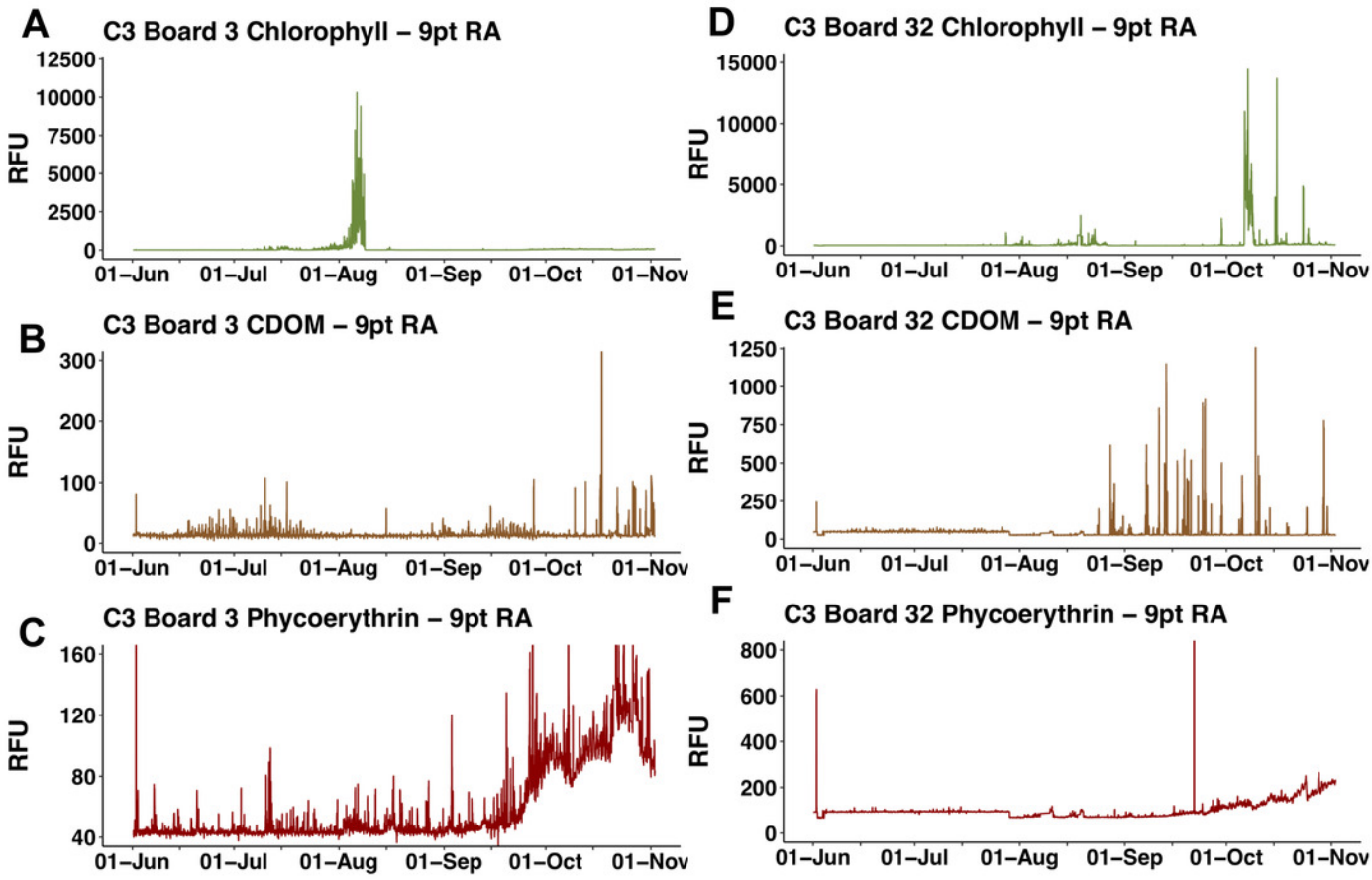

Figure 6

Processed holographic images of *Hemiaulus* and *Rhizosolenia* cells and aggregates.

(A) Curved chain of *Hemiaulus hauckii*. Each dark dot is the cell mass separated from adjacent cells by siliceous structures. Images have been contrast enhanced for clarity. (B) *Hemiaulus* aggregate. (C) *Hemiaulus* aggregate. (D) Two complete *Rhizosolenia* cells and half of the next cell with their symbionts *Richelia* (arrows) located at the apex of the cells.

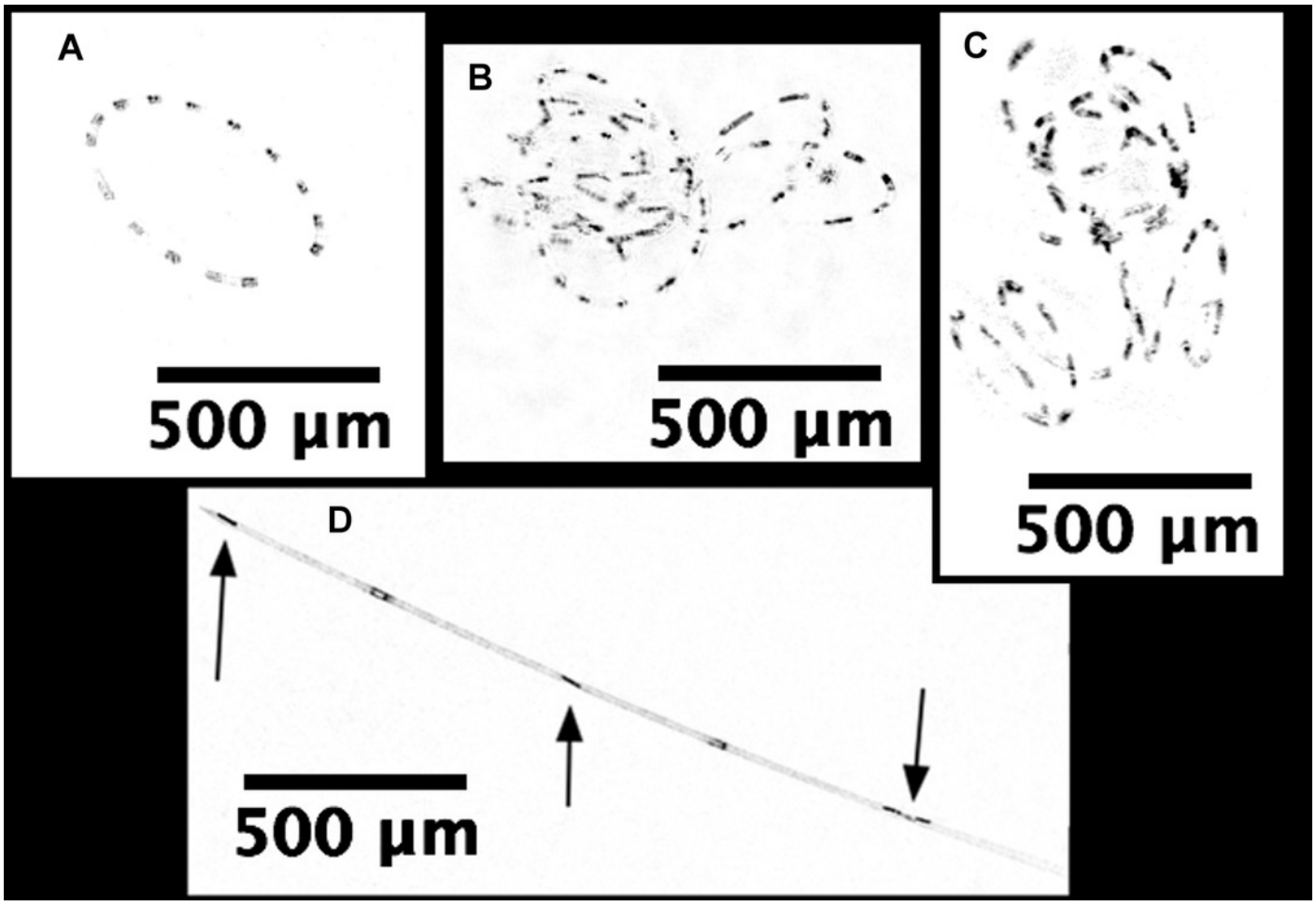

PeerJ Preprints NOT PEER-REVIEWED

Figure 7

Time series comparisons between the Aqua MODIS chl data and the *in situ* data collected by the *Honey Badger*'s sensors.

(A) 8-day composite data from Aqua MODIS showing surface chl concentrations (mg m^{-3}) near *Honey Badger*'s location. (B) *Hemiaulus* abundance (cells L^{-1}). (C) *Rhizosolenia* abundance (cells L^{-1}). (D) Biovolume from 11-58 µm bins. (E) Average F_v:$F_m$between 0800-1359 UTC (dark-adapted value). Blue and yellow shaded area indicate the *Hemiaulus* and *Rhizosolenia* bloom. respectively.

PeerJ Preprints NOT PEER-REVIEWED

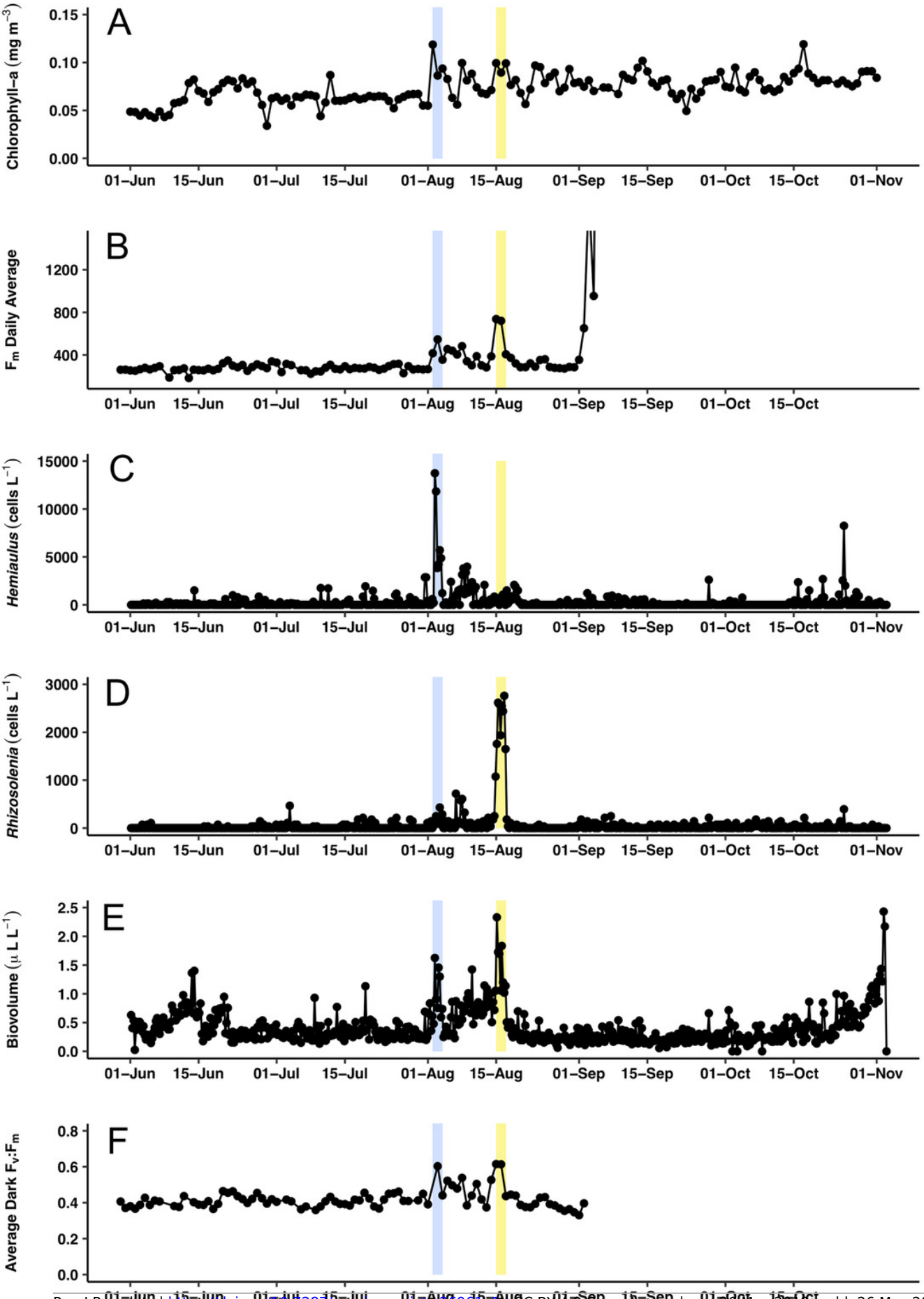

PeerJ Preprints NOT PEER-REVIEWED

Figure 8

Hemiaulus aggregated and free-living form distribution.

(A-B) Aqua MODIS chl surface concentration and *Honey Badger*'s position. Black dot= mission track position, red-white-black crosshair = *Honey Badger*'s position on day of satellite image. (A) 3 August 2015; *Hemiaulus* bloom B) 16 August 2015; *Rhizosolenia* bloom. (C) Time-series plot of *Hemiaulus* abundance in the free-living or aggregated form. (D) Locations of non-aggregated *Hemiaulus* cells and locations of aggregates. Red triangle = aggregate. Circles = non-aggregated *Hemiaulus* cells L^{-1}), size is proportional to abundance. The green area indicates where *Honey Badger* sampled during the SEP time window (15 July– 15 August).

PeerJ Preprints NOT PEER-REVIEWED

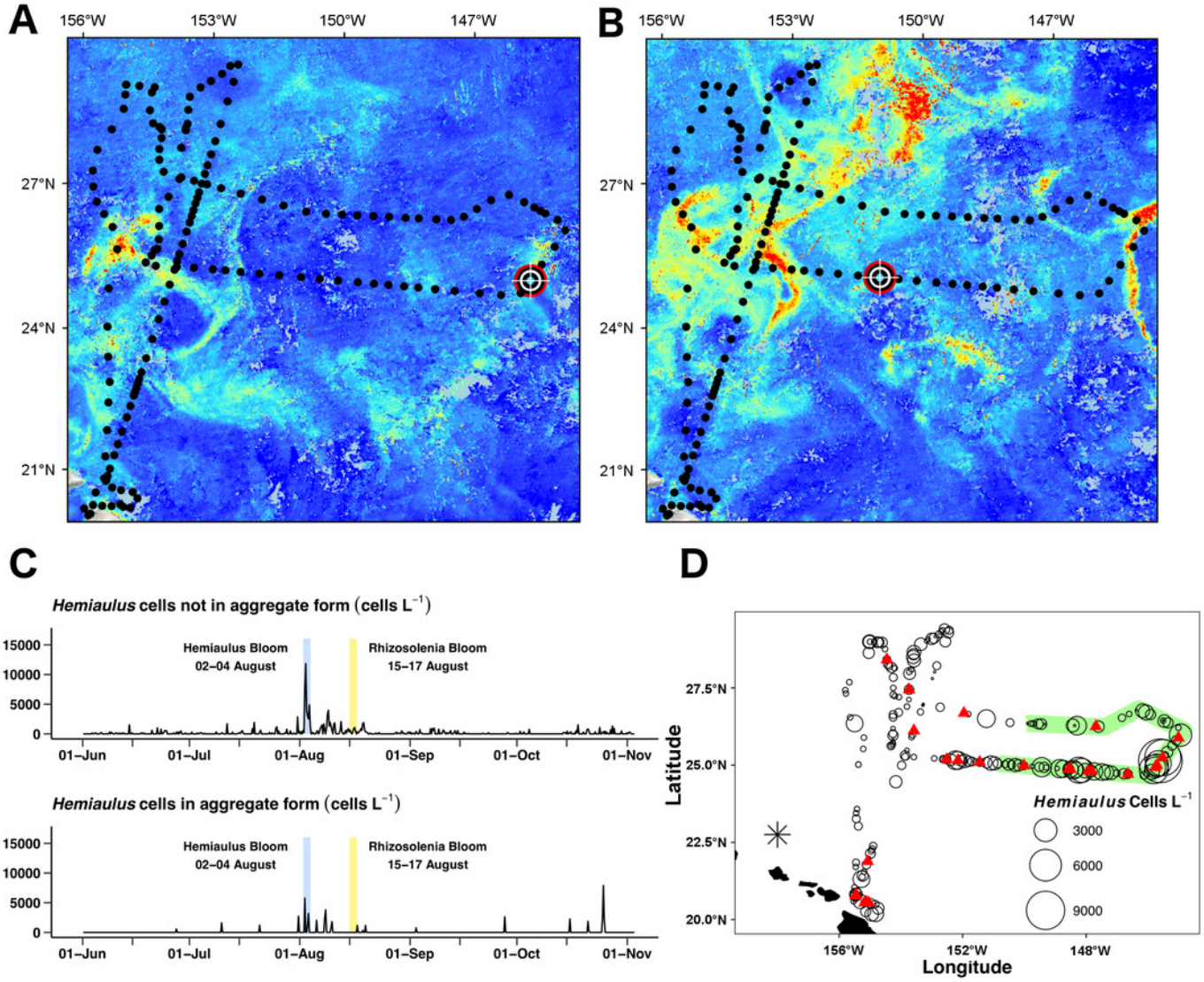

PeerJ Preprints NOT PEER-REVIEWED

Figure 9

PhytoFlash F_v:$F_m$diel rhythm sample and iron limitation index.

(A) Sample of the typical diel rhythm observed in the PhytoFlash F_v:$F_m$measurements. The signal is down-regulated during the daytime and returns to the maximum value during the dark period while macro-nutrient limited. Dark bars = 08:00-13:59 UTC (nocturnal period used in the calculation). Light bars = 18:00-02:59 UTC (diurnal period used in the calculation). (B) Time-series of the dark-averaged F_v:$F_m$minus the light-averaged F_v:F_m. Red points indicate where the sample number did not meet the threshold for calculation (see Methods). Asterisks are points where the data was compromised (see text).

PeerJ Preprints | https://doi.org/10.7287/peerj.preprints.26961v1 | CC BY 4.0 Open Access | rec: 26 May 2018, publ: 26 May 2018

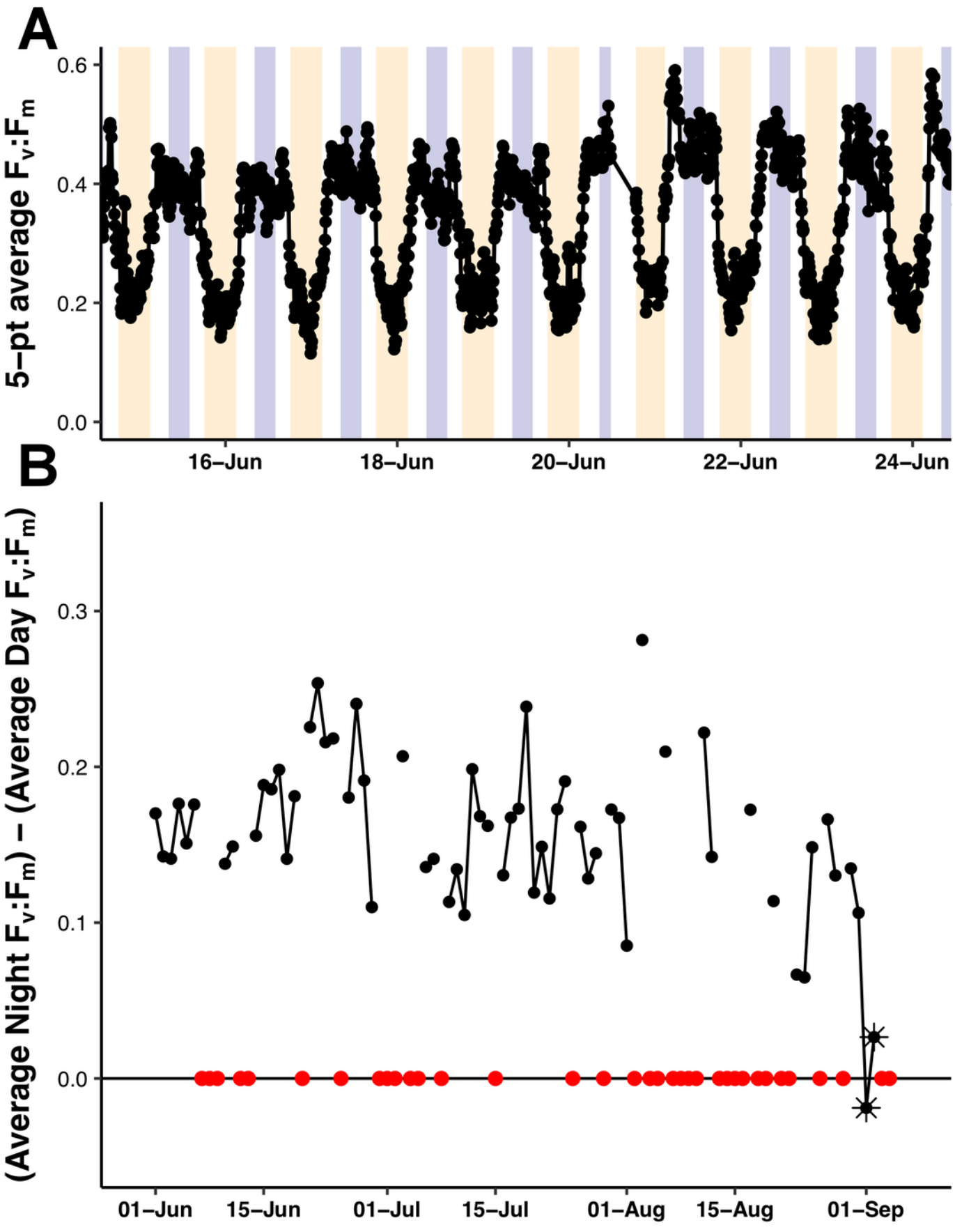
A
5–pt average F_v:F_m
0.6
0.4
0.2
0.0
16–Jun
18–Jun
20–Jun
22–Jun
24–Jun
B
(Average Night F_v:F_m) – (Average Day F_v:F_m)
0.3
0.2
0.1
0.0
01–Jun
15–Jun
01–Jul
15–Jul
01–Aug
15–Aug
01–Sep

PeerJ Preprints NOT PEER-REVIEWED

Table 1(on next page)

List of the instruments onboard the *Honey Badger* with their locations on the Wave Glider (Fig. 2) and their programmed sample frequency.

PeerJ Preprints NOT PEER-REVIEWED

1

Sensor (location)	Variables (units)	Interval	Available in Near Real Time?
Sea-Bird Scientific's gpCTD (2)	Water Temperature (°C), Salinity (PSU), Density (dBar)	48 hr^{-1}	Yes
Turner Designs' C3™ Submersible Fluorometer with Antifouling Coating (2)	Colored Dissolved Organic Mater (CDOM) (RFU), Chlorophyll-a (RFU), and Phycoerythrin Fluorescence (RFU)	6 hr^{-1}	Yes
Turner Designs' C3™ Submersible Fluorometer without Antifouling Coating (2)	Colored Dissolved Organic Mater (CDOM) (RFU), Chlorophyll-a (RFU), and Phycoerythrin Fluorescence (RFU)	6 hr^{-1}	Yes
AirMar Technology's WX Series Ultrasonic WeatherStation® (1)	Air Temperature (°C), Pressure (mBar), Average Wind Speed (knots) and Direction (degrees true)	6 hr^{-1}	Yes
Datawell BV's MOSE (2)	Significant wave height (m) and Direction (degrees true)	2 hr^{-1}	Yes
Cannon G10 Camera (2)	Downward facing camera for imaging the sub-body	6 hr^{-1}	No
Turner Designs' PhytoFlash (4)	F_o, F_m, F_v, Yield (F_v:F_m)	6 hr^{-1}	Yes
Sequoia Scientific LISST-Holo (5)	Holographic microscopic images of the water	1 burst of 15 images every 6 hr	No

2

PeerJ Preprints NOT PEER-REVIEWED

Table 2 (on next page)

Hemiaulus aggregate locations and contribution to total *Hemiaulus* abundance.

The *Hemiaulus* aggregate events outside (left) and within (right) the 15 July – 15 August SEP. N = number of aggregates in each 15 image burst at that location. The *Hemiaulus* bloom event is in bold, italicized text.

PeerJ Preprints NOT PEER-REVIEWED

1

Aggregate events outside the SEP					Aggregate Events within the SEP				
Date (UTC)	n	Location		*% Hemiaulus* in Aggregates (Total cells L^{-1})	Date (UTC)	n	Location		*% Hemiaulus* in Aggregates (Total cells L^{-1})
		°N	°N				°N	°W	
6/27/15 8:07	1	28.41	154.45	66.6 (861)	7/20/15 17:14	1	26.25	147.68	82.9 (1471)
7/10/15 1:06	1	26.69	151.96	91.8 (1757)	7/31/15 15:31	1	25.80	145.01	95.0 (2869)
8/17/15 4:01	1	25.10	151.45	78.6 (1506)	***8/02/15 10:09***	***3***	***25.24***	***145.52***	***42.0 (13737)***
8/18/15 16:37	1	25.15	152.15	15.5 (2080)	***8/03/15 4:29***	***1***	***25.00***	***145.71***	***29.7 (4232)***
8/19/15 10:55	1	25.18	152.51	78.6 (1506)	***8/03/15 10:38***	***3***	***24.93***	***145.76***	***56.0 (5702)***
9/2/15 16:29	1	27.44	153.74	64.7 (1219)	8/05/15 17:34	2	24.71	146.65	85.1 (2403)
9/27/15 14:14	1	26.12	153.58	100.0 (2618)	8/08/15 0:22	1	24.81	147.83	80.7 (3156)
10/15/15 21:22	1	21.80	155.08	95.5 (2367)	8/08/15 6:31	2	24.81	147.93	100.0 (3802)
10/20/15 23:22	2	20.81	155.46	69.3 (2690)	8/09/15 19:10	1	24.86	148.50	39.0 (2116)
10/21/15 5:28	1	20.77	155.47	31.8 (789)	8/10/15 1:10	1	24.87	148.57	75.8 (2367)
10/25/15 0:58	2	20.54	155.18	90.1 (2546)					
10/25/15 7:04	1	20.56	155.11	95.7 (8249)					
10/25/15 13:10	1	20.54	155.04	100.0 (2009)					

2

3